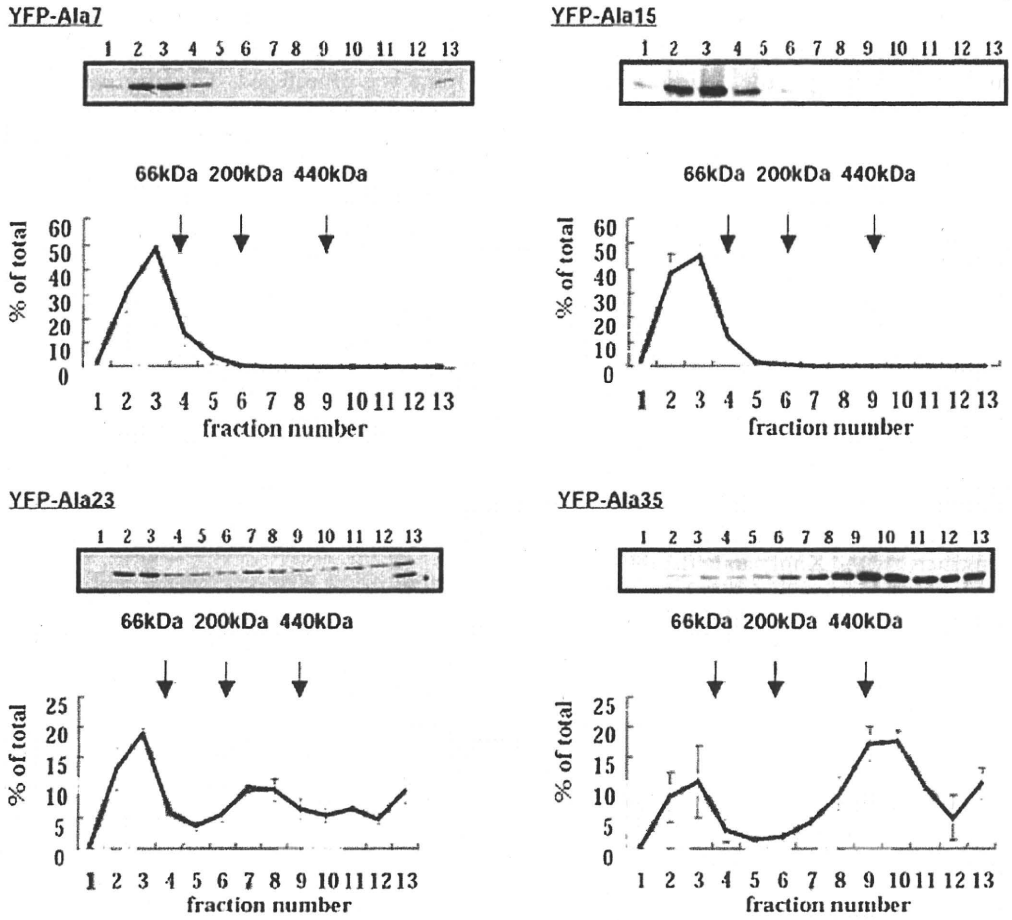

Fig. 1. Fractionation of YFP-Ala7, -Ala15, -Ala23, and -Ala35 by sucrose density gradient centrifugation. Proteins from whole COS-7 cells lysates were separated by sucrose density gradient centrifugation. Quantification of YFP-Ala proteins present in each fraction was determined by Western blotting with an anti-YFP antibody. The markers used for sucrose density centrifugation were: BSA (66 kDa), β-Amy (200 kDa), and ferritin (440 kDa). *Artificial degradation product.

PAGE by using purified GST-fusion proteins (GST-Ala7 to GST-Ala35). GST-Ala29 to GST-Ala35 products were retained in the upper part of the gel, whereas GST-Ala7 to GST-Ala23 products migrated into the running gel (Oma et al., 2007). We further investigated this difference by using sucrose density gradients. GST-Ala7, GST-Ala15, and GST-Ala23 were purified by using glutathione-Sepharose and subjected to sucrose density centrifugation. In contrast to GST-Ala35, these proteins sedimented in fractions 2–6 (Fig. 2). GST-Ala35 formed a huge complex just after purification, and the molecular species appeared to be heterogeneous.

Change in GST-Ala23 Conformation After Incubation at 37°C

The pathological length threshold of polyalanine tracts is thought to be about 20 residues. Cellular localization of polyalanine-containing proteins and oligomerization also changes at ~20 residues. However, in vitro oligomerization of GST-Ala occurs at a threshold of ~30 alanine residues (Oma et al., 2007). Therefore, we investigated changes in oligomerization of GST-fusion polyalanine-containing proteins containing ~20 residues. After dialysis against PBS, each protein was incubated at 37°C for 24 hr. All proteins migrated to their expected apparent molecular masses on SDS-polyacrylamide gels. However, by native PAGE, most GST-Ala23 protein that was incubated at 37°C for 24 hr was retained in the upper part of the running gel (Fig. 3A). In the presence of reducing agents, oligomerization of GST-Ala23 did not occur at all. The effect of reducing agents was not observed in GST-Ala35, which formed large aggregates.

These results suggest that GST-Ala23 formed an oligomer after incubation. Thus, we performed sucrose density gradient analysis to assess potential conformational changes in the protein. GST-Ala23 that was incubated at 37°C largely sedimented in fractions 1–13, whereas GST-Ala23 without incubation was concentrated in fractions 2–8 (Fig. 3B). These data suggest that

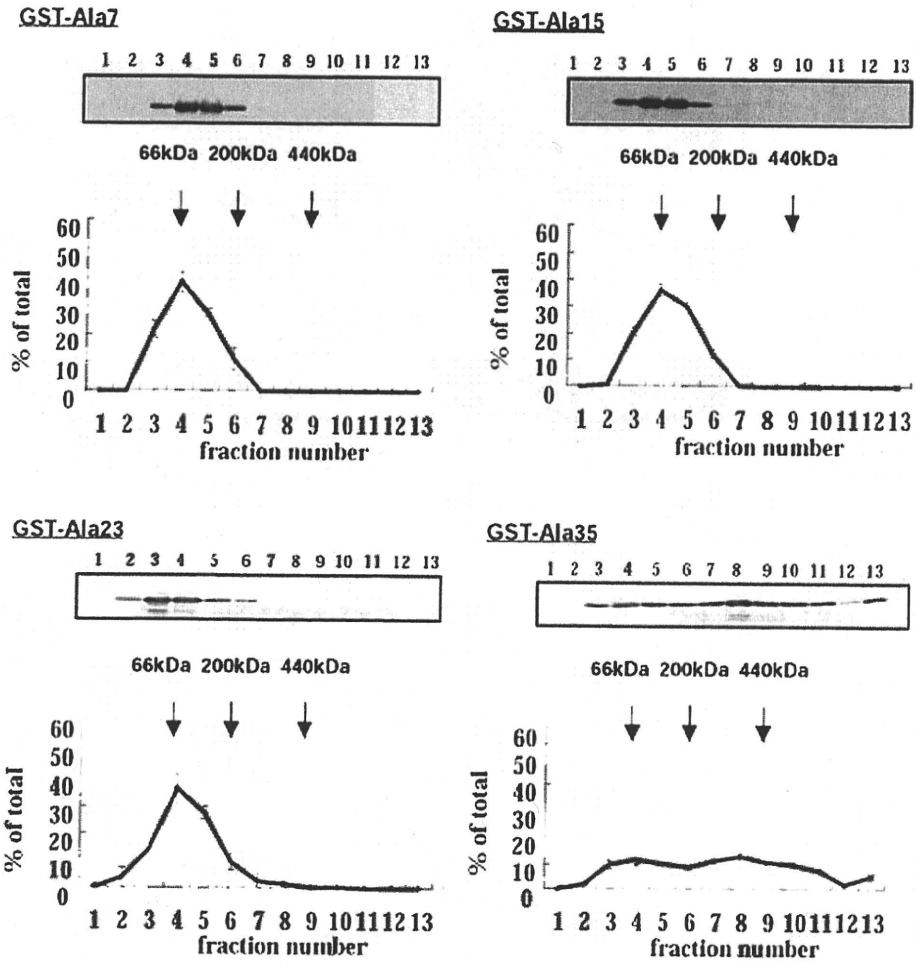

Fig. 2. Fractionation of purified GST-Ala7, -Ala15, -Ala23, and -Ala35 by sucrose density gradient centrifugation. Proteins were separated by sucrose density gradient centrifugation and quantified by Western blotting with an anti-GST antibody.

the differences in mobility on the native gel were due to oligomerization and that a huge complex formed after incubation.

Resistance of GST-Polyalanine Peptides to Trypsin Digestion

We next investigated the trypsin-mediated degradation rates of the long polyalanine repeat proteins. The degradation rate of GST-Ala35 was slower than that of GST-Ala7 (Fig. 4A,B); the $t_{1/2}$ was 50 min for GST-Ala7 and 210 min for GST-Ala35, respectively.

Resistance of GST-Ala23 to Trypsin Digestion

To determine whether resistance of the GST fusion protein to degradation by trypsin could be attributed to oligomerization, we investigated the degradation rate of GST-Ala23 that was allowed to oligomerize during long-term incubation at 37°C (Fig. 5A,B). The degradation rate of oligomerized GST-Ala23 was slower than that of nonoligomerized GST-Ala23.

Alteration of Trypsin Digestion After Fractionation

We further investigated the degradation rate of the GST fusion protein after fractionation by sucrose density centrifugation. In this experiment, GST-Ala35 was used because GST-Ala35 formed a huge complex without incubation (Fig. 2). Each fraction from the sucrose density gradient was incubated with trypsin (Fig. 6A,B). The degradation rate of GST-Ala35 was slower in the heavy fraction than in the light fraction. These data suggest that resistance to trypsin digestion is proportional to the size of the complex.

DISCUSSION

We investigated the oligomerization of proteins containing polyalanine repeats using YFP-Ala and GST-Ala. YFP-Ala proteins containing 23–35 alanine repeats were expressed in COS-7 cells, and they localized to the cytoplasm and nucleus (Oma et al., 2007). This localization was similar to that of pathological-length, homopo-

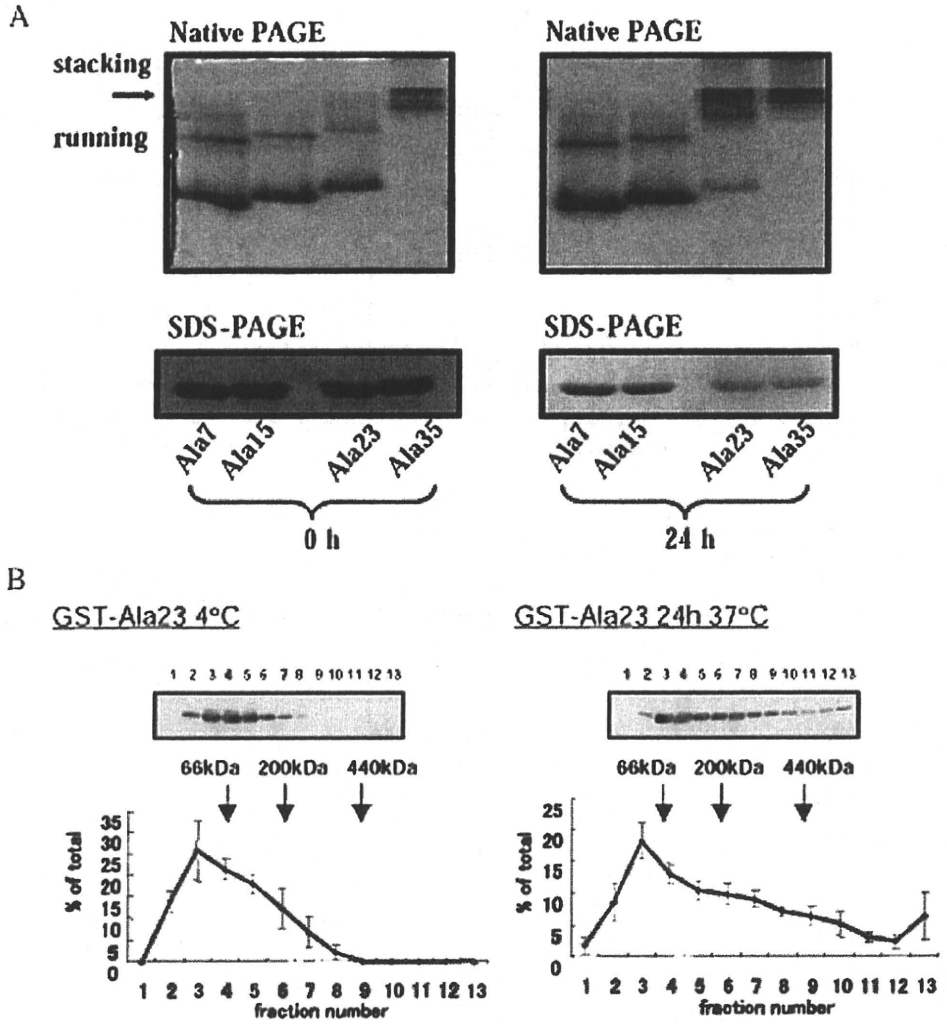

Fig. 3. Mobility shift of purified GST-Ala23 after long-term incubation. **A:** GST-Ala was incubated at 37°C for 24 hr and subjected to analysis by native- and SDS-PAGE. The proteins were stained with Coomassie brilliant blue. **B:** Fractionation of GST-Ala23 with or without long-term incubation by sucrose density gradient centrifugation. The amount of GST-Ala23 present in each fraction was assessed by Western blotting with an anti-GST antibody.

lymeric proteins such as Hoxd13, Hoxa13, Runx2, and Sox3 that were expressed in COS-1 cells (Albrecht et al., 2004). Because movement of proteins from the cytoplasm to the nucleus may be precluded by their oligomerization status, we analyzed the oligomerization of proteins containing polyalanine repeat tracts.

Our results showed that YFP-Ala23 and YFP-Ala35 oligomerized within the cells and that these proteins were heterogeneous in form. At a length considered to be pathological in polyalanine diseases, i.e., ~20 polyalanine residues, the proteins were unstable and were prone to oligomerization. Indeed, monomer to oligomer formation was recently reported for GFP-polyQ proteins expressed in COS cells (Takahashi et al., 2007). Collectively, these data suggest that the onset of polyglutamine and polyalanine diseases may relate to the oligomerization status of the disease-causing protein and that oligomerization itself is facilitated by the homopolymeric sequences. We previously found that polyalanine tracts were associated with mitochondria (Toriumi et al., 2008). Chaperone proteins such as Hsp40 and Hsp70 were also colocalized with aggregates formed by mutant PABPN1 having polyalanine expansion (Wang et al., 2005). Therefore, interacting proteins may be important for polyalanine oligomerization.

Proteins such as tumor necrosis factor-α (TNF-α) have short polyalanine repeats that make the protein resistant to degradation (Sharipo et al., 2001). Our studies show that oligomerized GST-fusion proteins are resistant to trypsin digestion and that large complexes are more resistant to trypsin digestion than smaller proteins. Furthermore, oligomerization of the proteins having long

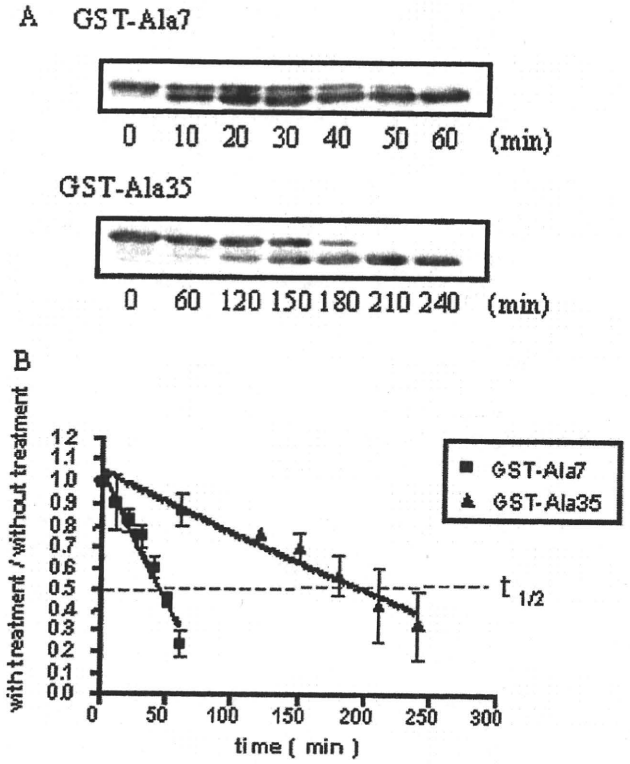

Fig. 4. Degradation of GST-polyalanine fusion proteins by trypsin. **A:** GST-fusion proteins with 7 and 35 polyalanine repeats were treated with trypsin for the indicated times, and the protein fragments were separated by SDS-PAGE, followed by Western blotting with an anti-GST antibody. **B:** Degradation rates of GST-Ala7 and -Ala35; the results shown are the means of three independent experiments ± SEM.

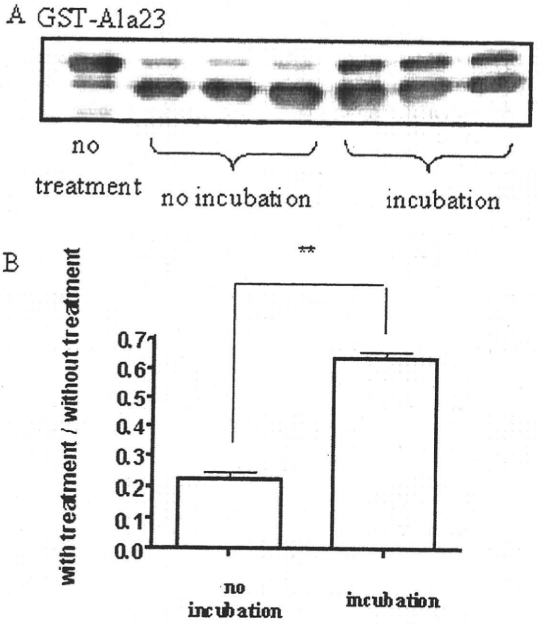

Fig. 5. Trypsin digestion of oligomerized GST-Ala23. **A:** Oligomerized GST-Ala23 was treated with trypsin for 1 hr, and the degradation rate of the protein was measured. Western blotting was performed using an anti-GST antibody. The assay was performed with three independent tubes to show the reproducibility. **B:** Quantification of the band intensities from three independent experiments. Values are the means ± SEM. $^{**}P < 0.01$ compared with GST-Ala23 without incubation. Student's two-tailed *t*-test.

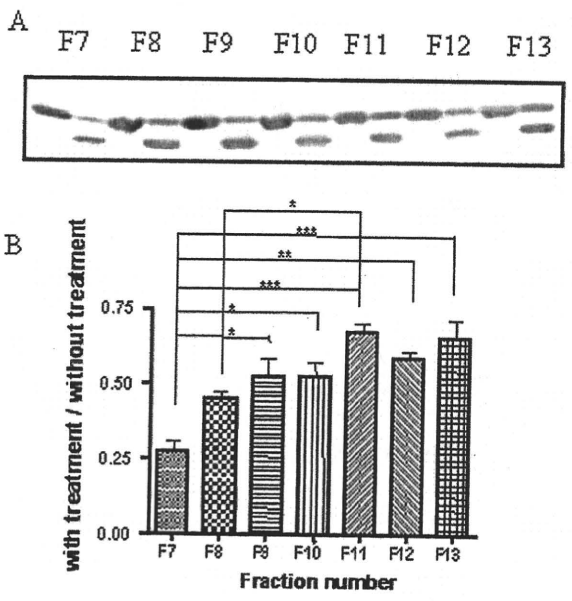

Fig. 6. Trypsin digestion of GST-Ala35. **A:** GST-Ala35 was left untreated (left) or treated (right) and separated by density gradient centrifugation. The proteins were then incubated with trypsin for 30 min, and Western blot analysis was performed with an anti-GST antibody. **B:** Quantification of the band intensities from three independent experiments. Values are means ± SEM. $^{*}P < 0.05$, $^{**}P < 0.01$, $^{***}P < 0.001$ compared with GST-Ala35 without treatment. ANOVA and post hoc Tukey's test were used as statistical tests.

polyalanine repeats prevented their translocation to the nucleus (Oma et al., 2007). Therefore, it is possible that oligomerized polyalanine repeat proteins in cytosol are toxic, because other fusion proteins that oligomerize as a result of excessive polyglutamine repeats, such as thioredoxin fusion protein, are toxic to cultured cells (Nagai et al., 2007).

After dialysis in the absence of reducing agents, GST-Ala23 oligomerized within 24 hr at 37°C. When reducing agents such as DTT were added to the solution, oligomerization did not occur. Therefore, reducing agents appear to inhibit oligomerization of homopolymeric proteins in vitro. We were unable to find other inhibitors. Candidate inhibitors that have been reported include Congo red (Heiser et al., 2000), polyglutamine binding peptide 1 (QBP1; Nagai et al., 2000), dimethylsulfoxide (DMSO), trimethylamine n-oxide (TMAO), and glycerol (Paul, 2007). Compounds that inhibit the common mechanisms that promote cellular toxicity resulting from homopolymeric repeats, e.g., oligomerization, are attractive therapeutic targets that warrant further study.

REFERENCES

Abu-Baker A, Messaed C, Laganiere J, Gaspar C, Brais B, Rouleau GA. 2003. Involvement of the ubiquitin-proteasome pathway and molecular chaperones in oculopharyngeal muscular dystrophy. Hum Mol Genet 12:2609–2623.

Alba MM, Guigo R. 2004. Comparative analyis of amino acid repeats in rodents and humans. Genome Res 14:549–554.

Albrecht A, Mundlos S. 2005. The other trinucleotide repeat: polyalanine expansion disorders. Curr Opin Genet Dev 15:285–293.

Albrecht AN, Kornak U, Boddrich A, Suring K, Robinson PN, Stiege AC, Lurz R, Stricker S, Wanker EE, Mundlos S. 2004. A molecular pathogenesis for transcription factor associated poly-alanine tract expansions. Hum Mol Genet 13:2351–2359.

Becher MW, Kotzuk JA, Davis LE, Bear DG. 2000. Intranuclear inclusions in oculopharyngeal muscular dystrophy contain poly(A) binding protein 2. Ann Neurol 48:812–815.

Dehay B, Bertolotti A. 2006. Critical role of the proline-rich region in huntingtin for aggregation and cytotoxicity in yeast. J Biol Chem 281:35608–35615.

Giri K, Bhattacharyya NP, Basak S. 2007. pH-dependent self-assembly of polyalanine peptides. Biophys J 92:293–302.

Heiser V, Scherzinger E, Boeddrich A, Nordhoff E, Lurz R, Schugardt N, Lehrach H, Wanker EE. 2000. Inhibition of huntingtin fibrillogenesis by specific antibodies and small molecules: implications for Huntington's disease therapy. Proc Natl Acad Sci USA 97:6739–6744.

Nagai Y, Tucker T, Ren H, Kenan DJ, Henderson BS, Keene JD, Strittmatter WJ, Burke JR. 2000. Inhibition of polyglutamine protein aggregation and cell death by novel peptides identified by phage display screening. J Biol Chem 275:10437–10442.

Nagai Y, Inui T, Popiel HA, Fujikake N, Hasegawa K, Urade Y, Goto Y, Naiki H, Toda T. 2007. A toxic monomeric conformer of the polyglutamine protein. Nat Struct Mol Biol 14:332–340.

Oma Y, Kino Y, Sasagawa N, Ishiura S. 2004. Intracellular localization of homopolymeric amino acid-containing proteins expressed in mammalian cells. J Biol Chem 279:21217–21222.

Oma Y, Kino Y, Toriumi K, Sasagawa N, Ishiura S. 2007. Interactions between homopolymeric amino acids (HPAAs). Prot Sci 16:2195–2204.

Paul S. 2007. Polyglutamine-mediated neurodegeneration: use of chaperones as prevention strategy. Biochemistry 72:359–366.

Rankin J, Wyttenbach A, Rubinsztein DC. 2000. Intracellular green fluorescent protein-polyalanine aggregates are associated with cell death. Biochem J 348:15–19.

Shanmugam V, Dion P, Rochefort D, Laganiere J, Brais B, Rouleau GA. 2000. PABP2 polyalanine tract expansion causes intranuclear inclusions in oculopharyngeal muscular dystrophy. Ann Neurol 48:798– 802.

Sharipo A, Imreh M, Leonchiks A, Brändén C, Masucci MG. 2001. cis-Inhibition of proteasomal degradation by viral repeats: impact of length and amino acid composition. FEBS Lett 499:137–142.

Shinchuk LM, Sharma D, Blondelle SE, Reixach N, Inouye H, Kirschner DA. 2005. Poly-(L-alanine) expansions form core beta-sheets that nucleate amyloid assembly. Proteins 61:579–589.

Takahashi Y, Okamoto Y, Popiel HA, Fujikake N, Toda T, Kinjo M, Nagai Y. 2007. Detection of polyglutamine protein oligomers in cells by fluorescence correlation spectroscopy. J Biol Chem 282:24039–24048.

Toriumi K, Oma Y, Kino Y, Futai E, Sasagawa N, Ishiura S. 2008. Expression of polyalanine stretches induces mitochondrial dysfunction. J Neurosci Res 86:1529–1537.

Wang Q, Mosser DD, Bag J. 2005. Induction of HSP70 expression and recruitment of HSC70 and HSP70 in the nucleus reduce aggregation of a polyalanine expansion mutant of PABPN1 in HeLa cells. Hum Mol Genet 14:3673–3684.

Neurochemistry International 54 (2009) 330–338

Contents lists available at ScienceDirect

Neurochemistry International

journal homepage: www.elsevier.com/locate/neuint

Proteomic and histochemical analysis of proteins involved in the dying-back-type of axonal degeneration in the gracile axonal dystrophy (*gad*) mouse

Akiko Goto [a,b], Yu-Lai Wang [a], Tomohiro Kabuta [a], Rieko Setsuie [a], Hitoshi Osaka [a], Akira Sawa [c], Shoichi Ishiura [b], Keiji Wada [a,*]

[a] Department of Degenerative Neurological Diseases, National Institute of Neuroscience, National Center of Neurology and Psychiatry, 4-1-1 Ogawahigashi, Kodaira, Tokyo, 187-8502, Japan
[b] Department of Life Sciences, Graduate School of Arts and Sciences, University of Tokyo, 3-8-1 Komaba, Meguro-ku, Tokyo,153-8902, Japan
[c] Depts. of Psychiatry and Neuroscience, Johns Hopkins University School of Medicine, Baltimore, MD 21287, USA

ARTICLE INFO

Article history:
Received 24 November 2008
Received in revised form 12 December 2008
Accepted 17 December 2008
Available online 25 December 2008

Keywords:
Axonal degeneration
Dying-back
gad mouse
UCH-L1
Ubiquitin
2D-DIGE
GAPDH
Oxidative stress

ABSTRACT

Local axonal degeneration is a common pathological feature of peripheral neuropathies and neurodegenerative disorders of the central nervous system, including Alzheimer's disease, Parkinson's disease, and stroke; however, the underlying molecular mechanism is not known. Here, we analyzed the gracile axonal dystrophy (*gad*) mouse, which displays the dying-back-type of axonal degeneration in sensory neurons, to find the molecules involved in the mechanism of axonal degeneration. The *gad* mouse is analogous to a null mutant of ubiquitin carboxyl-terminal hydrolase L1 (UCH-L1). UCH-L1 is a deubiquitinating enzyme expressed at high levels in neurons, as well as testis and ovary. In addition, we recently discovered a new function of UCH-L1—namely to bind to and stabilize mono-ubiquitin in neurons, and found that the level of mono-ubiquitin was decreased in neurons, especially in axons of the sciatic nerve, in *gad* mice. The low level of ubiquitin suggests that the target proteins of the ubiquitin proteasome system are not sufficiently ubiquitinated and thus degraded in the *gad* mouse; therefore, these proteins may be the key molecules involved in axonal degeneration. To identify molecules involved in axonal degeneration in *gad* mice, we compared protein expression in sciatic nerves between *gad* and wild-type mice at 2 and 12 weeks old, using two-dimensional difference gel electrophoresis. As a result, we found age-dependent accumulation of several proteins, including glyceraldehyde-3-phosphate dehydrogenase (GAPDH) and 14-3-3, in *gad* mice compared with wild-type mice. Histochemical analyses demonstrated that GAPDH and 14-3-3 were localized throughout axons in both *gad* and wild-type mice, but GAPDH accumulated in the axons of *gad* mice. Recently, it has been suggested that a wide range of neurodegenerative diseases are characterized by the accumulation of intracellular and extracellular protein aggregates, and it has been reported that oxidative stress causes the aggregation of GAPDH. Furthermore, histochemical analysis demonstrated that sulfonated GAPDH, a sensor of oxidative stress that elicits cellular dysfunction, was expressed in the axons of *gad* mice, and 4-hydroxy-2-nonenal, a major marker of oxidative stress, was also only detected in *gad* mice. Our findings suggest that GAPDH may participate in a process of the dying-back-type of axonal degeneration in *gad* mice and may provide valuable insight into the mechanisms of axonal degeneration.

1. Introduction

Axonal degeneration occurs in several chronic neurodegenerative diseases and in injuries caused by, for example, toxic, ischemic, or traumatic insults. Recent findings suggest that axonal degeneration precedes, and sometimes causes, neuronal death in these neurodegenerative disorders (Li et al., 2001; Ferri et al., 2003; Fischer et al., 2004; Stokin et al., 2005; Fischer and Glass, 2007), but the underlying molecular mechanism is not known.

The gracile axonal dystrophy (*gad*) mutant mouse is characterized by sensory ataxia at an early stage, followed by motor ataxia at a later stage (Yamazaki et al., 1988; Saigoh et al., 1999). Pathologically, axonal degeneration in the *gad* mouse begins with the distal ends of primary ascending axons in the dorsal root ganglia (DRG) (Mukoyama et al., 1989; Kikuchi et al., 1990; Oda et al., 1992; Miura et al., 1993), and spheroid formation in the dying-back-type of axonal degeneration is observed in the gracile and dorsal spinocerebellar tracts (Yamazaki et al., 1988; Kikuchi

* Corresponding author. Tel.: +81 42 346 1715 fax: +81 42 346 1745.
E-mail address: wada@ncnp.go.jp (K. Wada).

0197-0186/$ – see front matter © 2008 Elsevier Ltd. All rights reserved.
doi:10.1016/j.neuint.2008.12.012

et al., 1990; Miura et al., 1993). At a later stage, axonal degeneration and spheroid formation are observed at both the central and peripheral ends of DRG neurons and extend transsynaptically to the upper tracts as well as to motor neurons (Mukoyama et al., 1989; Kikuchi et al., 1990; Oda et al., 1992; Miura et al., 1993). Therefore, the *gad* mouse is an effective model for analyzing the molecular mechanism of the dying-back-type of axonal degeneration.

Previously, we found that the *gad* mutation is caused by an in-frame deletion of *Uchl1*, which encodes ubiquitin carboxyl-terminal hydrolase L1 (UCH-L1) (Saigoh et al., 1999). UCH-L1 is expressed at high levels in neurons, as well as testis and ovary, and constitutes ~5% of total soluble protein in the brain (Wilkinson et al., 1989). UCH-L1 is reported to be one of the deubiquitinating enzymes in the ubiquitin-proteasome system (UPS), where it hydrolyzes bonds between ubiquitin (Ub) and small adducts and creates free mono-Ub *in vitro* (Larsen et al., 1998). UCH-L1 also acts as a Ub ligase *in vitro* (Liu et al., 2002). In addition, we recently found a new function for UCH-L1—to bind to and stabilize mono-Ub in neurons (Osaka et al., 2003).

Using histochemical analysis, we previously demonstrated that UCH-L1 and mono-Ub are colocalized in axons of the sciatic nerve. In *gad* mice, the level of mono-Ub was decreased in neurons, especially in axons of the sciatic nerve (Osaka et al., 2003). The low level of ubiquitin suggests that the target proteins of the ubiquitin-proteasome system (UPS) are not sufficiently ubiquitinated and thus degraded in the *gad* mouse; therefore, these proteins may be key molecules involved in axonal degeneration. To identify the molecules involved in axonal degeneration in *gad* mice, we analyzed protein expression in sciatic nerves using two-dimensional difference gel electrophoresis (2D-DIGE).

Proteomic approaches compare protein expression comprehensively; 2D-DIGE is a modification of the traditional 2D technology, in which small amounts of multiple protein samples can be compared together, because each sample can be pre-labeled with different fluorescence dyes, mixed together, and run on the same isoelectric focusing (IEF) gel and SDS-PAGE (Knowles et al., 2003; Shaw and Riederer, 2003). We used 2D-DIGE because it is the most efficient method for analyzing the small amount of protein that can be extracted from a sciatic nerve. Here, we show that there are age-dependent accumulations of several proteins, including glyceraldehyde-3-phosphate dehydrogenase (GAPDH) and 14-3-3, in *gad* mice compared with wild-type (WT) mice, suggesting that these proteins are involved in axonal degeneration.

2. Experimental procedures

2.1. Animals

We used homozygous *gad* mice and their wild-type siblings (Harada et al., 2004; Wang et al., 2004). Mice were maintained and propagated at the National Institute of Neuroscience, National Center of Neurology and Psychiatry, Japan. Proteomic studies were carried out at 2 and 12 weeks old. Western blotting analyses were carried out at 12 weeks old. Histochemical analyses were carried out at 7 and 12 weeks old. Animals were anesthetized with Nembutal, and the sciatic nerve was perfused with saline. All mouse experiments were performed in accordance with our institution's regulations for animal care and with the approval of the Animal Investigation Committee of the National Institute of Neuroscience, National Center of Neurology and Psychiatry which conforms to the National Institute of Health guide for the care and use of laboratory animals.

2.2. Preparation of protein samples and labeling of protein samples with Cy dyes

Each sciatic nerve was suspended in 300 μl of sample buffer, containing 7 M urea, 2 M thiourea, 4% (w/v) CHAPS, and 40 mM Tris base (pH 8.0), by sonication for 60 s on ice, gently vortexed, and centrifuged for 20 min at 14,000 × *g* at 4 °C. Protein concentration was determined using a 2-D Quant Kit (GE Healthcare, Piscataway, NJ, USA). Protein samples were labeled as recommended by the manufacturer (GE Healthcare) using 400 pmol Cy dyes (GE Healthcare) per 50 μg of protein. Separate solutions containing 15 μg of protein from one *gad* or WT sample were labeled with Cy3 or Cy5 dye, respectively, and a common pool of proteins with *gad* and WT samples mixed equally were labeled with Cy2 dye by vortexing and incubating on ice in the dark for 30 min. The labeled samples were quenched by the addition of 1 μl 10 mM lysine (Sigma–Aldrich, St. Louis, MO, USA) and incubated on ice for 10 min.

2.3. Two-dimensional polyacrylamide gel electrophoresis (2D PAGE)

The quenched Cy3, Cy5, and Cy2 samples (15 μg of protein each) were mixed and denatured in 2D PAGE sample buffer containing 7 M urea, 2 M thiourea, 4% (w/v) CHAPS, 0.2% DTT, and 1.4% Ampholine. For the IEF, 45 μg of protein was applied to a rehydrated Immobiline Drystrip (pH 3–10, 7 cm; GE Healthcare) in a strip holder and incubated overnight in the dark. IEF was performed using a Multiphor II Electrophoresis system (GE Healthcare). The electrophoresis conditions were set as follows: step 1, 200 V for 1 min; step 2, 3500 V for 90 min; step 3, 3500 V for 125 min. After IEF, the strip was equilibrated with SDS buffer and applied to the 12.5% 2D SDS-PAGE for the analysis of 12-week-old mice and to the 4–20% SDS-PAGE for the analysis of 2-week-old mice using a precast Multigel II system (Daiichi Kagaku, Japan).

2.4. Image analysis and statistics

We scanned 2D gels using a Typhoon 9000 fluorescent imager (GE Healthcare). Excitation/emission wavelengths were chosen for each of the dyes. Gel images were preprocessed to remove extraneous areas using ImageQuant V5.0 (GE Healthcare). Gel analysis was performed using DeCyder DIA V5.0 (Difference In-gel Analysis; GE Healthcare). In-gel matching and statistical analysis were performed using DeCyder BVA V5.0 (Biological Variance Analysis; GE Healthcare). The Student's paired *t*-test ($P < 0.05$) was performed to identify the protein spots that were differentially expressed between *gad* and WT mice.

2.5. In-gel digestion and analysis by matrix-assisted laser desorption/ionization tandem time-of-flight (MALDI-TOF/TOF) mass spectrometry

To identify a particular protein in a spot detected by 2D-DIGE analysis, sciatic nerve extract containing 100 μg of protein was subjected to 12.5% 2D SDS-PAGE and stained with Coomassie brilliant blue (Invitrogen). The spots of interest were excised from the gel, destained, dehydrated with acetonitrile for 10 min, and completely dried under a vacuum pump for 10 min. Each spot was placed in 20 μl of 5 mM NH_4HCO_3 containing 1 pmol of sequencing-grade trypsin (Promega, Madison, WI, USA) overnight at 37 °C. Aliquots of the trypsinized samples were analyzed by nanoliquid chromatography and automatically spotted with alpha-cyano-4-hydroxy-cinnamic acid solution on a stainless-steel target and air dried. All mass spectra were obtained with MALDI-TOF/TOF (AXIMA-CFR; Shimadzu, Japan). MALDI peptide spectra were calibrated using several peaks of self-digested trypsin and matrix ion as internal standards.

2.6. Protein identification

Protein identification was performed using database searches on the web with Mascot Wizard (Matrix Science Ltd., London, United Kingdom). Criteria for protein identification were as follows: mascot score higher than 80 and mass tolerance of 100 ppm. Calculated pI and molecular mass data were obtained by Mascot.

2.7. 2D Western blotting for identification of GAPDH

One protein spot that was increased in *gad* mice but could not be detected by MALDI-TOF/TOF analysis was speculated to be GAPDH from its isoelectric point, molecular weight and location of the 2D gel compared with the mouse brain proteome database, and was therefore subjected to 2D Western blotting using an anti-GAPDH antibody (1:200, Chemicon, MAB374). One-hundred μg of sciatic nerve proteins were separated by 12.5% 2D SDS-PAGE and transferred onto a PVDF membrane (Immobilon-P; Millipore, Bedford, MA, USA). The membrane was washed with MilliQ water for 1 h at room temperature. Western blotting was performed as described in the following section.

2.8. Western blotting

Using 4–20% gradient SDS-PAGE, 2 μg of total protein was separated and transferred onto a PVDF membrane (Immobilon-P; Millipore). The membrane was washed with MilliQ water, then blocked with 5% skim milk in 0.05% Tween 20 in TBS (TTBS) for 1 h at room temperature, and incubated with primary antibodies in TTBS overnight at 4 °C. Primary antibodies used in this study were anti-UCH-L1 polyclonal antibody (1:5000, UltraClone, RA95101), anti-GAPDH monoclonal antibody (1:200, Chemicon, MAB374), anti-14-3-3 polyclonal antibody (1:100, IBL, 18649), anti-neurofilament L monoclonal antibody (NF-L, 1:500, Chemicon, MAB1615), anti-neuronal class III β tubulin antibody (βTUBIII, 1:1000, Covance, TUJ1), and anti-actin monoclonal antibody (1:4000, Sigma, AC-15). After washing, the membranes were incubated for 1 h at room temperature with either anti-mouse or anti-rabbit IgG horseradish peroxidase (HRP) conjugated secondary antibodies (1:10,000, GE Healthcare). Protein signals were detected with SuperSignal West Femto Maximum Sensitivity Substrate (Pierce) and were visualized with the LAS-3000 imaging system (Fujifilm, Tokyo, Japan).

2.9. Immunohistochemistry

Mice were anesthetized and perfused with ice-cold 4% paraformaldehyde in phosphate-buffered saline (PBS, pH 7.4). Sciatic nerves were collected and postfixed in 4% paraformaldehyde overnight at 4 °C. The samples were embedded in paraffin and sectioned at 5 μm for immunohistochemistry. Serial sections were deparaffinized in xylene and graded ethanol, and washed in distilled water. Sections were blocked by incubation in 10% normal goat serum for 30 min at room temperature and incubated overnight at 4 °C with diluted primary antibodies. The following antibodies were used at the final dilutions indicated: anti-GAPDH polyclonal antibody (1:1000), anti-sulfonated GAPDH polyclonal antibody (1:500; these two antibodies were kindly provided by Dr. Sawa), anti-14-3-3 polyclonal antibody (1:100, IBL, 18649), anti-myelin basic protein monoclonal antibody (MBP, 1:200, QED Bioscience, 24201), anti-neurofilament M monoclonal antibody (NF-M, 1:200, Chemicon, MAB1621), anti-UCH-L1 polyclonal antibody (1:2000, UltraClone, RA95101), anti-UCH-L1 monoclonal antibody (1:200; Medac, Wedel, Germany), βTUBIII (1:300, COVANCE, TUJ1), and anti-4-hydroxy-2-nonenal monoclonal antibody (HNE, 25 μg/ml, JaICA, Shizuoka, Japan).

After incubating with primary antibodies, sections were washed 5 times with 0.1% Tween 20 in PBS (PBST) for 5 min at room temperature and then incubated for 90 min at room temperature with diluted secondary antibodies. The following antibodies were used at the final dilutions indicated: anti-mouse-Alexa594 IgG and anti-rabbit-Alexa588 IgG (1:400, Invitrogen) for immunofluorescence staining, or EnVision+ anti-rabbit HRP (Dako, Japan) for DAB staining. For DAB staining, bound antibody complexes were visualized using DAB (Dako, Japan) as a peroxidase substrate. Primary and secondary antibodies were diluted in Dako Antibody Diluent (Dako, Japan). After incubation with secondary antibodies, sections were washed 5 times with PBST for 5 min at room temperature and mounted with Antifade Kit (Molecular Probes). For analysis of 14-3-3 and HNE, sections were pretreated in a microwave oven for 10 min in citrate buffer solution (pH 6.0), cooled down, and washed 3 times for 5 min in PBS at room temperature. For the other immunostaining analyses, this pretreatment was not needed. For DAB staining, sections were treated with 3% H_2O_2 in methanol for 5 min to quench endogenous peroxidase activity before treatment with the primary antibodies.

3. Results

3.1. Analyses of differentially expressed proteins between gad and WT mice by 2D-DIGE

To find proteins that are upregulated in *gad* mice compared with WT mice, we analyzed sciatic nerves from 3 *gad* and 3 WT mice at 2 weeks old as well as at 12 weeks old, using 2D-DIGE technology. The proteins from *gad* mice were pre-labeled with Cy5 (red), and the proteins from WT mice were pre-labeled with Cy3 (green), respectively. A common pool of proteins composed of an equal amount of protein from a single *gad* and WT mouse was pre-labeled with Cy2, and the same manipulation was performed in 3 independent experiments.

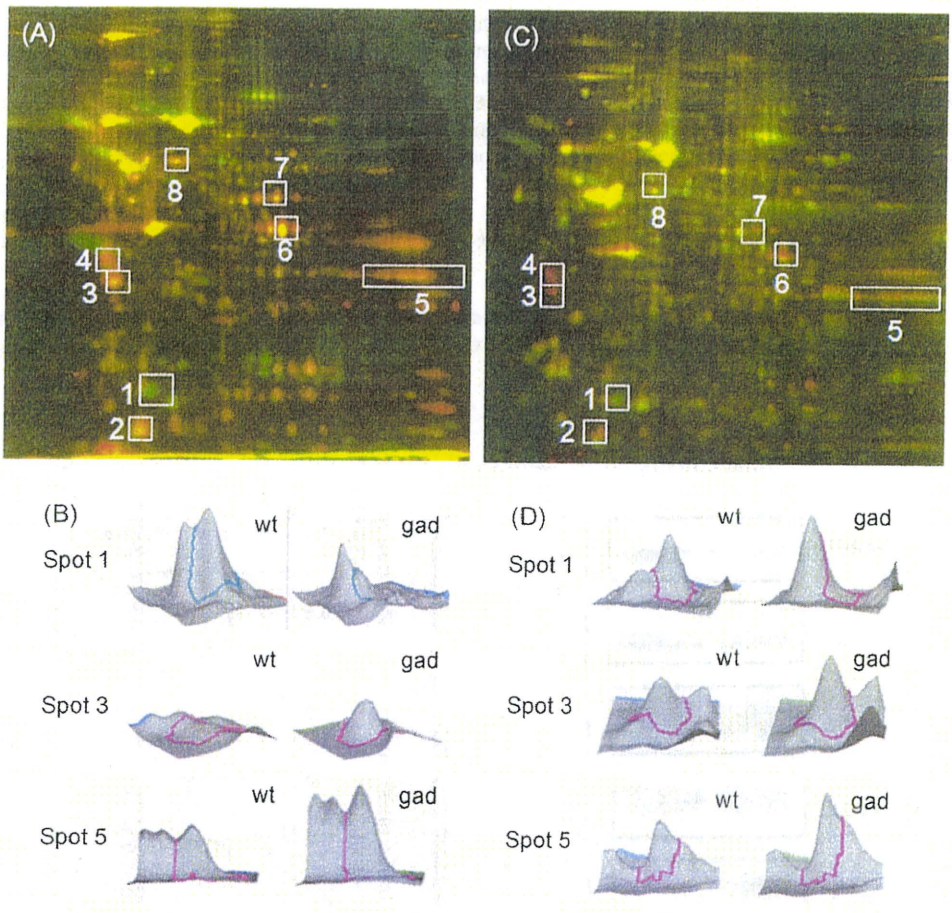

Fig. 1. Analyses of differentially expressed proteins between *gad* and wild-type mice by two-dimensional difference gel electrophoresis (2D-DIGE).
(A) A representative pseudocolor picture of superimposed DIGE images of mice at 12 weeks old. Fourteen protein spots are increased in *gad* mice compared with wild-type (WT) mice (red) by at least 1.6-fold (Student's paired *t*-test value; $P < 0.05$ in 3 parallel gels), and one spot is not detected at all in *gad* mice (green). Seven protein spots (spot No. 2–8) are increased in *gad* mice in an age-dependent manner, and one spot (spot No. 1) was not detected at all in *gad* mice at either 2 or 12 weeks old. The spot numbers of the latter differentiated 8 spots are shown in this map.
(B) A representative pseudocolor picture of superimposed DIGE images of mice at 2 weeks old. Eighteen protein spots are increased in *gad* mice compared with WT mice (red) by at least 1.6-fold (Student's paired *t*-test value; $P < 0.05$ in 3 parallel gels), and one spot is not detected at all in *gad* mice (green). The spot numbers in this figure are the same as in A.
(C) The 3D images of typical protein spots that were differentially expressed between *gad* and WT mice at 2 weeks old (spot numbers 1, 3, and 5 in A).
(D) The 3D images of typical protein spots that were differentially expressed between *gad* and WT mice at 2 weeks old (spot numbers 1, 3, and 5 in C) (For interpretation of the references to color in this figure legend, the reader is referred to the web version of the article.)

Table 1
List of proteins differentially expressed between *gad* and WT mice.

Spot no.	Protein name	Score	Molecular mass (kDa)/pI	Av. ratio (*gad*/wt) 12 weeks	*P* value	Av. ratio (*gad*/wt) 2 weeks	*P* value
1	Ubiquitin thiolesterase PGP9.5 (UCH-L1)	96	25.10/5.12	−14.38	0.005	−3.89	0.003
3	14-3-3 protein	94	28.10/4.63	5.4	0.030	7.32	0.001
4	Annexin A5	143	35.79/4.83	6.68	0.020	5.19	0.030
8	Neurofilament triplet L protein (NF-L)	212	61.40/4.62	2.18	0.010	3.53	0.026
5	Glyceraldehyde 3-phosphate dehydrogenase (GAPDH)		38.07/8.34	3.89	0.043	1.61	

*GAPDH was detected by 2D Western blotting and not by MALDI-TOF/TOF.

Fig. 1A shows a representative pseudocolor picture of superimposed DIGE images of the 12-week-old mouse samples. Fourteen protein spots were increased by at least 1.6-fold in *gad* mice compared with WT mice (red; Student's paired *t*-test value; $P < 0.05$ in 3 parallel gels), and one spot was not detected at all in *gad* mice (green).

Fig. 1B shows a representative pseudocolor picture of superimposed DIGE images of the 2-week-old mouse samples. Eighteen protein spots were increased by at least 1.6-fold in *gad* mice compared with WT mice (red; Student's paired *t*-test value; $P < 0.05$ in 3 parallel gels), and one spot was not detected at all in *gad* mice (green).

Based on comparison of the 2D-DIGE analysis of mice between 2 and 12 weeks old, 7 protein spots showed an age-dependent increase in *gad* mice (spots No. 2–8). One spot (spot No. 1) was not detected at all in *gad* mice at either 2 or 12 weeks old (Fig. 1A and B).

Fig. 1C shows the 3D images of typical spots (spots No. 1, 3, and 5) in Fig. 1A, and Fig. 1D shows the 3D images of typical spots (spots No. 1, 3, and 5) in Fig. 1B.

3.2. Identification of differentially expressed proteins between gad and WT mice by MALDI-TOF/TOF and 2D Western blotting

The proteins of spots that were age dependently increased or absent in *gad* mice were analyzed by MALDI-TOF/TOF and identified (spots No. 1, 3, 4, and 8). The proteins were identified as UCH-L1 (spot No. 1), 14-3-3 (spot No. 3), annexin V (spot No. 4), and Neurofilament L (NF-L) (spot No. 8). Additionally, we speculated that spot No. 5 may represent GAPDH based on the information from the mouse brain proteome database (http://www.charite.de/humangenetik/klose_public1/index.html), and confirmed this by 2D Western blotting with GAPDH antibodies. The results of the protein identification are listed in Table 1, including spot number, protein name, mascot score, theoretical relative molecular mass, isoelectric point, average ratio of *gad*/wt protein level, and *P*-value using DeCyder, at both 2 and 12 weeks old.

3.3. Analyses of the expression levels of proteins in gad and WT mice by Western blotting

In 2D-DIGE system, each sample was pre-labeled with different fluorescence dyes, Cy3, Cy5 or Cy2. This labeling-process allows comparison of multiple samples in same 2D-gel, but it is reported that efficiency of each dyes to label proteins was not exactly the same. We assume that 2D-DIGE is reliable method to detect molecules involved in axonal degeneration but Western blot analysis using specific antibodies is more accurate, and in fact, it is usual that identified proteins by TOF-MASS are reconfirmed by Western blotting. Therefore, the expression levels of the proteins in

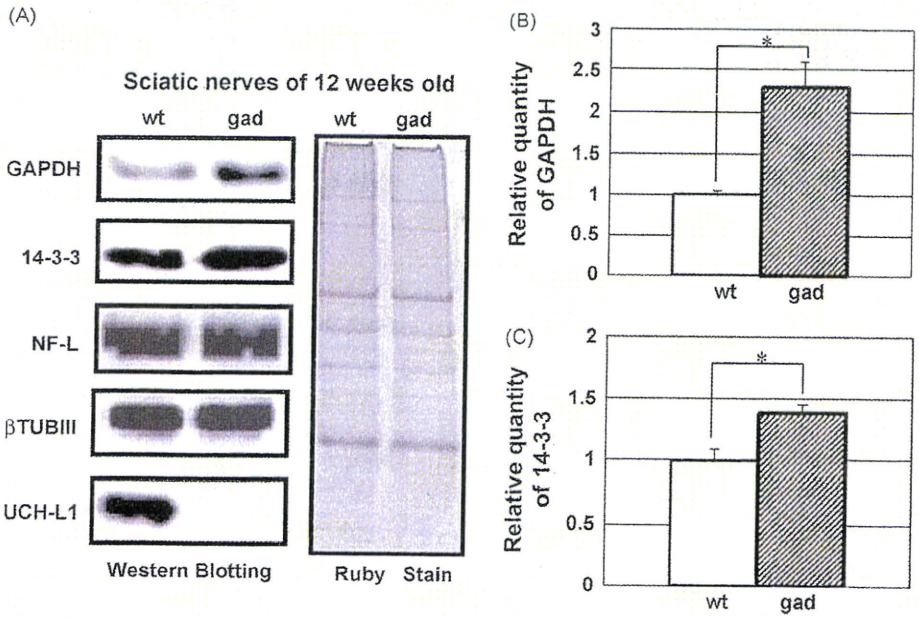

Fig. 2. Western blotting analyses of the expression levels of proteins expressed differentially between *gad* and WT mice.
(A) Results of Western blotting analysis with antibodies against ubiquitin carboxyl-terminal hydrolase L1 (UCH-L1), neurofilament L (NF-L), 14-3-3, glyceraldehyde-3-phosphate dehydrogenase (GAPDH), and classIII β tubulin (βTUBIII). GAPDH and 14-3-3 protein levels were increased in *gad* mice compared with WT mice.
(B) Quantification of the band intensities of GAPDH. Values are means ± SEM of 3 independent experiments ($^*P < 0.05$); GAPDH is increased by about 2.3-fold in *gad* mice at 12 weeks old compared with WT mice.
(C) Quantification of the band intensities of 14-3-3. Values are means ± SEM of 3 independent experiments ($^*P < 0.05$); 14-3-3 is increased by 1.3-fold in *gad* mice at 12 weeks old compared with WT mice.

gad and WT mice listed in Table 1 were further analyzed by Western blotting to reconfirm the results of 2D-DIGE (Fig. 2A). We chose these proteins because they were all reported to be expressed in neurons. In 12-week-old *gad* mice, GAPDH was increased by an average ratio of 2.3-fold (Fig. 2B), and 14-3-3 was increased by an average ratio of 1.3-fold (Fig. 2C) compared with WT mice. The levels of NF-L and βTUBIII, which was used as an internal control, showed no significant difference between *gad* and WT mice at 12 weeks old (Fig. 2A). Annexin V was not analyzed because its antibodies did not work in this experimental system containing urea and thiourea. The same results were obtained in 3 independent experiments.

3.4. Histochemical localization of GAPDH in the sciatic nerves of gad and WT mice

Sciatic nerves are composed internally of neuronal axons and externally of myelin derived from glial Schwann cells, and protein samples in the proteomic analysis were a mixture of axons and myelin. We examined the histological localization of GAPDH, which was dominantly increased in *gad* mice, by double immunofluorescence staining using an antibody against GAPDH and the neuronal markers neurofilament M (NF-M) or UCH-L1, or the Schwann cells marker myelin basic protein (MBP). In *gad* mice, GAPDH was colocalized with MBP (Fig. 3A, right panel) but was more dominantly colocalized with NF-M, a neuronal marker (Fig. 3A, left panel). These results suggest that GAPDH is mainly localized in axons in *gad* mice. In WT mice, GAPDH was colocalized with the neuronal marker UCH-L1 (Fig. 3B, left panel). Because UCH-L1 is the product of the gene defective in the *gad* mouse, UCH-L1 is not detected in *gad* mice (Fig. 3B, right panel). The same results were obtained in 3 independent experiments.

3.5. DAB staining analyses of GAPDH and 14-3-3 in the sciatic nerves of gad and WT mice

We examined in detail the localization of GAPDH in cross or vertical sections of sciatic nerve axons by DAB staining (Figs. 4A–F). In the cross-sections, GAPDH was localized in axons in both *gad* and WT mice and was remarkably accumulated in *gad* mice compared with WT mice (Fig. 4A and B). In vertical sections, GAPDH was also localized in axons in both *gad* and WT mice (Fig. 4C–F). Notably, aggregates of GAPDH were observed in *gad* mice but not in WT mice (Fig. 4E and F, arrow). Next, we examined the expression of 14-3-3, which was found to be increased in *gad* mice upon 2D-DIGE and Western blotting analyses. In both *gad* and WT mice, 14-3-3 was expressed in axons, and there was no significant difference between *gad* and WT mice (Fig. 4G–J). The same results were obtained in 3 independent experiments.

3.6. Histochemical analyses of sulfonated GAPDH in the sciatic nerves of gad and WT mice

It was reported that oxidative stress induces the oligomerization and aggregation of GAPDH (Cumming and Schubert, 2005; Nakajima et al., 2007), and in this study we found that GAPDH is accumulated in axons of *gad* mice that exhibit a dying-back-type of axonal degeneration. Thus, we postulated that oxidative stress would be increased in *gad* mice, and therefore examined the expression of sulfonated GAPDH (Hara et al., 2005), in the sciatic

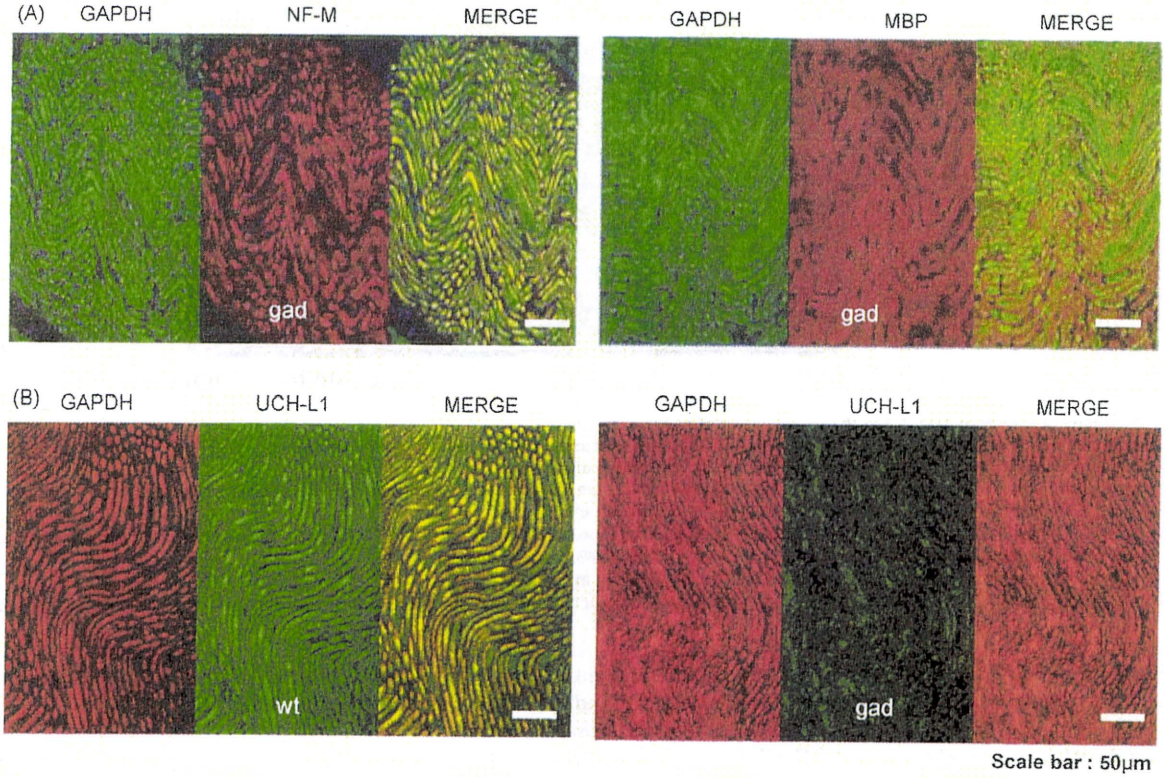

Fig. 3. Histochemical localization of GAPDH in the sciatic nerves of *gad* and WT mice.
(A) Double immunofluorescent staining of the sciatic nerve of *gad* mice using antibodies against GAPDH, neurofilament M (NF-M), or myelin basic protein (MBP). GAPDH was colocalized with NF-M (left panel) and partly with MBP (right panel) in *gad* mice. GAPDH is mainly localized in axons.
(B) Double immunofluorescent staining of the sciatic nerve of *gad* and WT mice using antibodies against GAPDH and UCH-L1. In WT mice, GAPDH is colocalized with UCH-L1 (left panel). In *gad* mice, UCH-L1 is not detected (right panel), and GAPDH is strongly detected compared with WT mice.

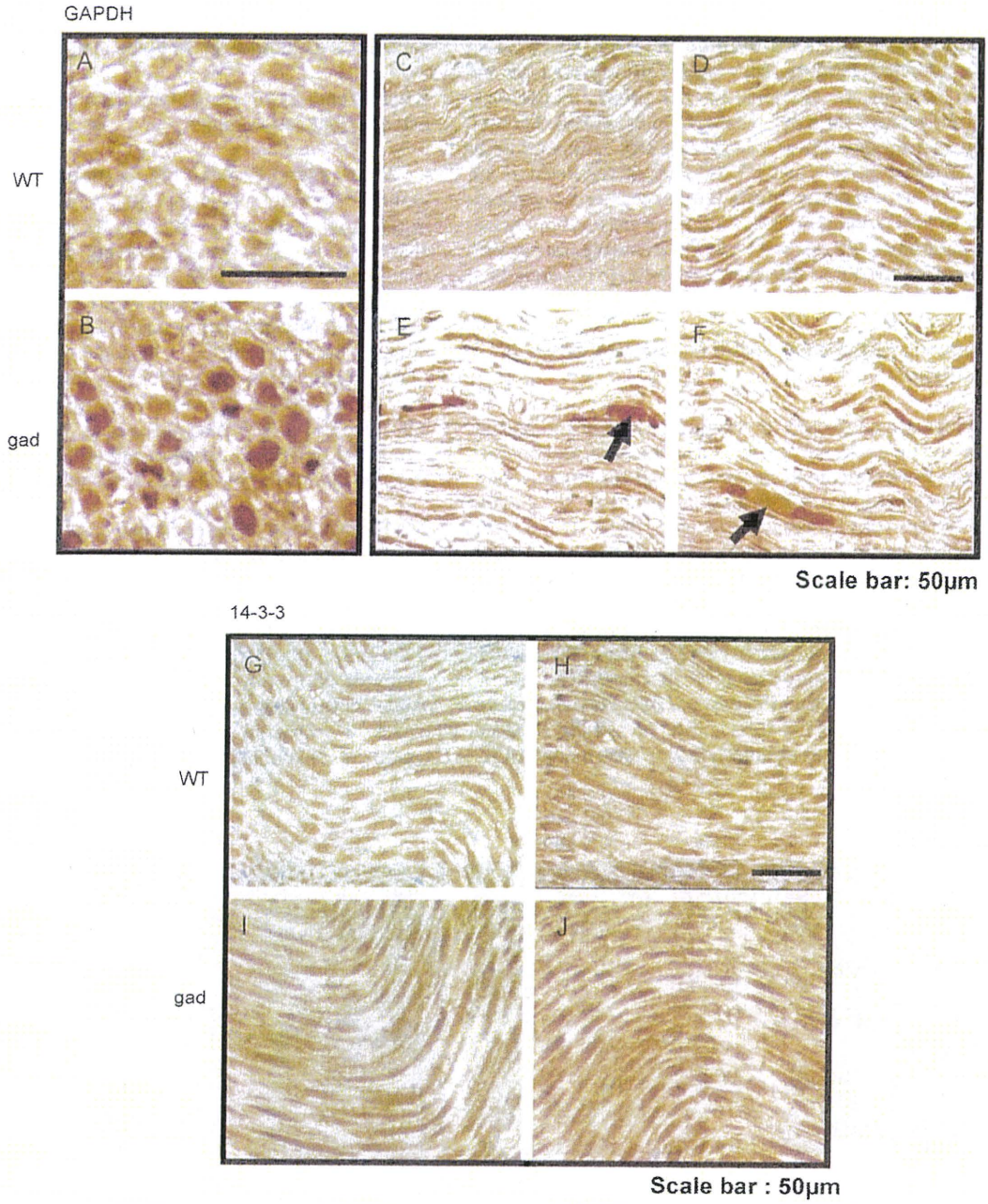

Fig. 4. DAB staining of GAPDH and 14-3-3 in the sciatic nerves of *gad* and WT mice.
(A–F) Sections of sciatic nerves of WT (A, C, and D) or *gad* (B, E, and F) mice stained with DAB using GAPDH antibodies.
(A) Cross-section of a sciatic nerve of a WT mouse. GAPDH is mainly localized in axons.
(B) Cross-section of a sciatic nerve of a *gad* mouse. GAPDH is mainly localized in axons and is highly expressed compared with the WT mouse.
(C and D) Vertical sections of sciatic nerves of WT mice. GAPDH is localized in axons.
(E and F) Vertical sections of sciatic nerves of *gad* mice. GAPDH is localized in axons and is accumulated. GAPDH aggregates are indicated by arrows.
(G–J) Sections of sciatic nerves of WT (G, H) and *gad* (I, J) mice stained with DAB using 14-3-3 antibodies.
(G and H) Vertical sections of sciatic nerves of WT mice; 14-3-3 is localized in axons of WT mice.
(I and J) Vertical sections of sciatic nerves of *gad* mice; 14-3-3 is localized in axons of *gad* mice, and there was no significant difference between *gad* and WT mice (G, H).

nerves of *gad* and WT mice. We found that although sulfonated GAPDH was not detected in WT mice, it was clearly detected in *gad* mice (Fig. 5A and B). In *gad* mice, sulfonated GAPDH was colocalized with the neuronal markers βTUBIII (Fig. 5B) and NF-M (data not shown) in axons. In *gad* mice, accumulated sulfonated GAPDH was also detected in the outer portion of the axons, around the DAPI staining for nuclei (Fig. 5C). Axons do not contain nuclei, so these DAPI signals may come from Schwann cells. The same results were obtained in 3 independent experiments.

3.7. Histological analyses of HNE, a marker of oxidative stress, in the sciatic nerves of gad and WT mice

The results shown in Fig. 5 suggest that the level of oxidative stress is increased in *gad* mice. Accordingly, we examined the existence of HNE, a major marker of oxidative stress, in addition to sulfonated GAPDH. HNE was detected in *gad* mice, but not in WT mice (Fig. 6). The same results were obtained in 3 independent experiments.

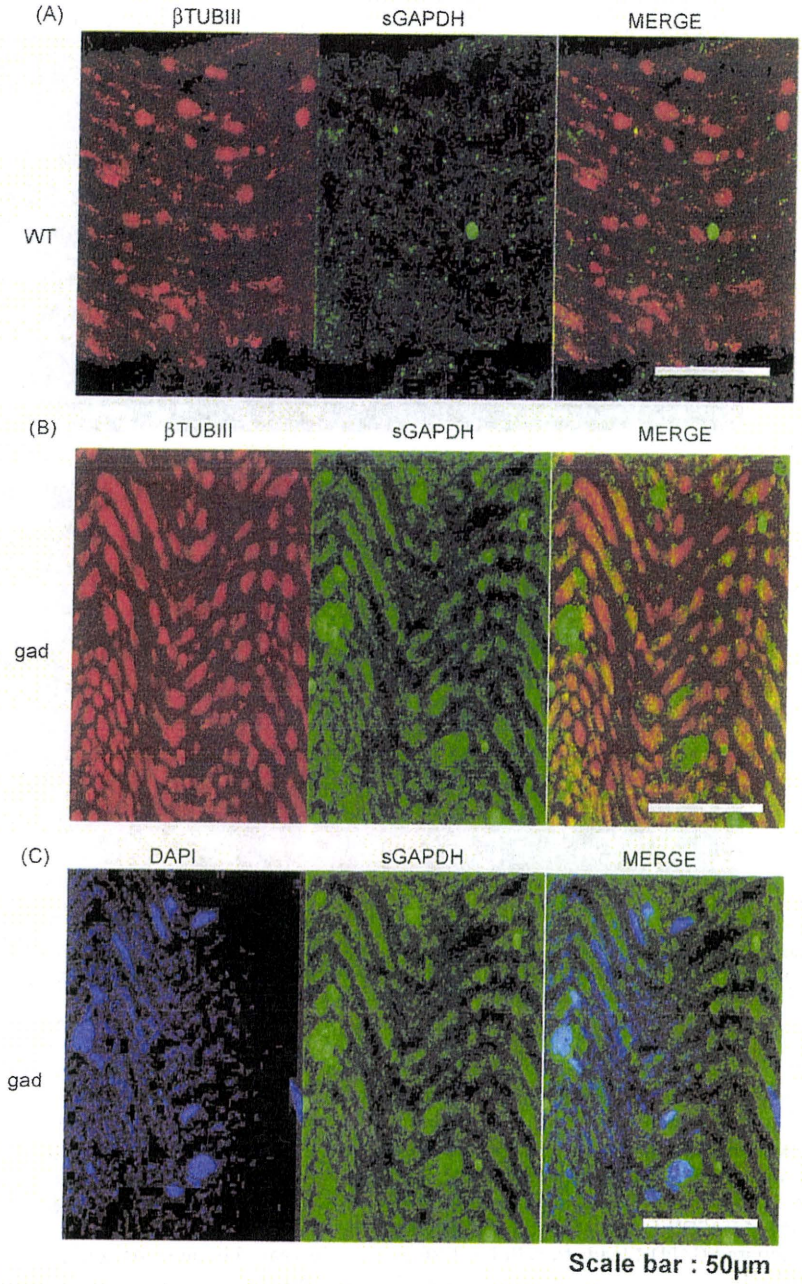

Fig. 5. Expression of sulfonated GAPDH in the sciatic nerves of *gad* and WT mice.
(A) Double immunofluorescent staining of a sciatic nerve of a WT mouse using antibodies against sulfonated GAPDH and βTUBIII. Sulfonated GAPDH was not detected in WT mice (middle panel).
(B) Double immunofluorescent staining of a sciatic nerve of a *gad* mouse using antibodies against sulfonated GAPDH and βTUBIII. In *gad* mice, sulfonated GAPDH was detected in axons of sciatic nerves (middle panel). Sulfonated GAPDH was colocalized with the neuronal marker βTUBIII in *gad* mice (right panel), as well as NF-M (data not shown). A representative result from 3 independent experiments is shown.
(C) Double immunofluorescent staining of a sciatic nerve of the *gad* mouse using an antibody against sulfonated GAPDH and DAPI. Sulfonated GAPDH was detected uniformaly within the axons of *gad* mice, and accumulation of sulfonated GAPDH was detected around the DAPI signals (right panel).

4. Discussion

In this study, we found that 14-3-3, annexin V, NF-L, and GAPDH were increased in an age-dependent manner in *gad* mice that display the dying-back-type of axonal degeneration, using 2D-DIGE analyses (Fig. 1). Based on Western blotting analyses, 14-3-3 and GAPDH were increased in *gad* mice compared with WT mice (Fig. 2). Histochemical analysis revealed that GAPDH was localized throughout axons and was accumulated in axons in *gad* mice compared with WT mice (Figs. 3 and 4). Also 14-3-3 was localized throughout axons, but there was no significant difference between *gad* and WT mice upon histochemical analyses, although it was increased in *gad* mice upon Western blotting analyses (Fig. 4). Since Western blotting showed only a slight increase in 14-3-3 (Fig. 2), we assume that this small difference could not be detected by histochemical analyses.

GAPDH is a classic glycolytic enzyme (Sirover, 1999; Chuang et al., 2005), and recent studies show that it is multifunctional

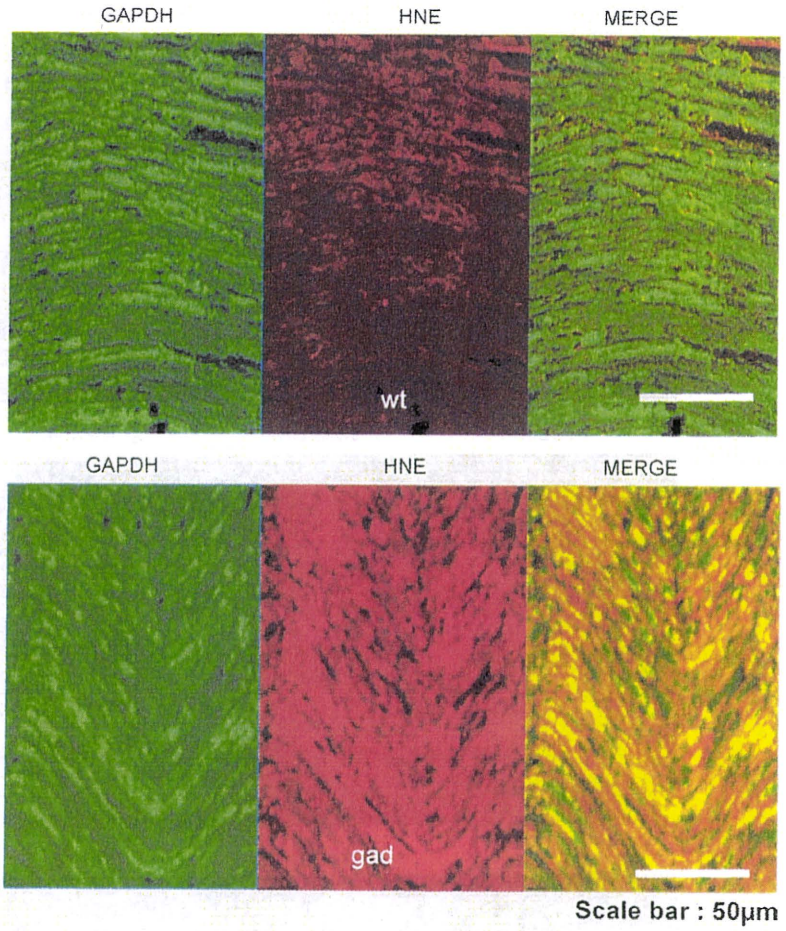

Fig. 6. Expression of HNE, a marker of oxidative stress, in the sciatic nerves of *gad* and WT mice.
Double immunofluorescent staining of sciatic nerves of *gad* and WT mice using antibodies against GAPDH and HNE. In WT mice, HNE was not detected (upper panel). On the other hand, HNE was strongly detected and mainly colocalized with GAPDH in *gad* mice (lower panel).

(Hara et al., 2006a). GAPDH has been reported to play roles in membrane fusion, microtubule bundling, nuclear RNA transport (Sirover, 1999), and transcription (Zheng et al., 2003). Particularly, its role as a mediator for cellular dysfunction/death has been highlighted (Sawa et al., 1997; Ishitani et al., 1998; Hara et al., 2005, 2006b). Sulfonation of GAPDH is reported to be induced by oxidative stress, and sulfonated GAPDH leads to cellular dysfunction (Hara et al., 2005, 2006a; Sen et al., 2008). Additionally, oxidative stress induces the oligomerization and aggregation of GAPDH through aberrant disulfide bonding of active-site cysteines, which leads to the formation of insoluble aggregates *in vitro* (Cumming and Schubert, 2005; Nakajima et al., 2007). Thus, GAPDH appears to participate in the mechanism leading to cellular dysfunction/death induced by oxidative stress. However, its function in axons or its association with axonal degeneration has not yet been demonstrated.

In this study, we found that GAPDH and sulfonated GAPDH were accumulated in *gad* mice compared with WT mice, suggesting that oxidative stress is increased in *gad* mice. In fact, we found that the oxidative stress marker HNE is increased in *gad* mice. It has also been reported that, the levels of carbonyl modification of proteins that is caused by oxidative stress are increased in the brains of *gad* mice compared with WT mice (Castegna et al., 2004). Therefore, we assume that accumulation of GAPDH and sulfonated GAPDH in the axons of *gad* mice were induced by oxidative stress.

Various molecules are involved in reduction-oxidative reactions, and recently the necessity of the UPS in reduction-oxidative reactions has been highlighted (Okada et al., 1999; Kang et al., 2008). It has been reported that a number of oxidative stress sensors are regulated by the UPS (Iwai, 2003; Kobayashi et al., 2004; Hara et al., 2006a). In *gad* mice, free-Ub pools are decreased in neurons, and proteolysis in the UPS is thought to be abnormal (Osaka et al., 2003). Oxidative stress is therefore expected to be increased in *gad* mice, which is consistent with our findings.

There is another possible mechanism for the accumulation of GAPDH in the axons of *gad* mice. GAPDH is reported to be degraded mainly by chaperone-mediated autophagy (Aniento et al., 1993; Cuervo et al., 1997). Our recent study showed that UCH-L1 physically interacts with lysosome-associated membrane protein type 2A, which is a component of CMA (Kabuta et al., 2008); thus CMA is possibly altered in the neuronal system of *gad* mice, potentially leading to the accumulation of GAPDH in the axons of *gad* mice.

This study demonstrates the alteration of GAPDH in axons of the *gad* mouse, a mutant with a loss of function of UCH-L1. Our findings suggest that GAPDH may participate in the process leading to the dying-back-type of axonal degeneration in *gad* mice and may provide valuable insight into the mechanisms of axonal degeneration.

Acknowledgements

We thank the following people for their contributions to this work: Dr. Hidemitsu Nakajima (Osaka Prefecture University), Dr. Satoshi Nagamine (National Center of Neurology and Psychiatry) and Dr. Makoto R. Hara (Johns Hopkins University School of Medicine) for helpful discussions; Ms. Hisae Kikuchi (National Center of Neurology and Psychiatry) for technical assistance with tissue sections; Ms. Masako Shikama (National Center of Neurology and Psychiatry) for the care and breeding of animals; Dr. Hayato Onishi (University of Tokyo) for assistance with the TOF MASS analysis; and Dr. H. Akiko Popiel (National Center of Neurology and Psychiatry) for support with English; Mitsubishi Tanabe Pharma Corporation for giving a chance to A.G. of admission to doctoral course. This work was supported in part by Grants-in-Aid for Scientific Research from the Ministry of Health, Labour and Welfare of Japan, Grants-in-Aid for Scientific Research from the Ministry of Education, Culture, Sports, Science and Technology of Japan, the Program for Promotion of Fundamental Studies in Health Sciences of the National Institute of Biomedical Innovation, and a grant from Japan Science and Technology Agency.

References

Aniento, F., Roche, E., Cuervo, A.M., Knecht, E., 1993. Uptake and degradation of glyceraldehyde-3-phosphate dehydrogenase by rat liver lysosomes. J. Biol. Chem. 268, 10463–10470.

Castegna, A., Thongboonkerd, V., Klein, J., Lynn, B.C., Wang, Y.L., Osaka, H., Wada, K., Butterfield, D.A., 2004. Proteomic analysis of brain proteins in the gracile axonal dystrophy (gad) mouse, a syndrome that emanates from dysfunctional ubiquitin carboxyl-terminal hydrolase L-1, reveals oxidation of key proteins. J. Neurochem. 88, 1540–1546.

Chuang, D.M., Hough, C., Senatorov, V.V., 2005. Glyceraldehyde-3-phosphate dehydrogenase, apoptosis, and neurodegenerative diseases. Annu. Rev. Pharmacol. Toxicol. 45, 269–290.

Cuervo, A.M., Dice, J.F., Knecht, E., 1997. A population of rat liver lysosomes responsible for the selective uptake and degradation of cytosolic proteins. J. Biol. Chem. 272, 5606–5615.

Cumming, R.C., Schubert, D., 2005. Amyloid-beta induces disulfide bonding and aggregation of GAPDH in Alzheimer's disease. FASEB J. 19, 2060–2062.

Ferri, A., Sanes, J.R., Coleman, M.P., Cunningham, J.M., Kato, A.C., 2003. Inhibiting axon degeneration and synapse loss attenuates apoptosis and disease progression in a mouse model of motoneuron disease. Curr. Biol. 13, 669–673.

Fischer, L.R., Culver, D.G., Tennant, P., Davis, A.A., Wang, M., Castellano-Sanchez, A., Khan, J., Polak, M.A., Glass, J.D., 2004. Amyotrophic lateral sclerosis is a distal axonopathy: evidence in mice and man. Exp. Neurol. 185, 232–240.

Fischer, L.R., Glass, J.D., 2007. Axonal degeneration in motor neuron disease. Neurodegener. Dis. 4, 431–442.

Hara, M.R., Agrawal, N., Kim, S.F., Cascio, M.B., Fujimuro, M., Ozeki, Y., Takahashi, M., Cheah, J.H., Tankou, S.K., Hester, L.D., Ferris, C.D., Hayward, S.D., Snyder, S.H., Sawa, A., 2005. S-nitrosylated GAPDH initiates apoptotic cell death by nuclear translocation following Siah1 binding. Nat. Cell. Biol. 7, 665–674.

Hara, M.R., Cascio, M.B., Sawa, A., 2006a. GAPDH as a sensor of NO stress. Biochim. Biophys. Acta 1762, 502–509.

Hara, M.R., Thomas, B., Cascio, M.B., Bae, B.I., Hester, L.D., Dawson, V.L., Dawson, T.M., Sawa, A., Snyder, S.H., 2006b. Neuroprotection by pharmacologic blockade of the GAPDH death cascade. Proc. Natl. Acad. Sci. U.S.A. 103, 3887–3889.

Harada, T., Harada, C., Wang, Y.L., Osaka, H., Amanai, K., Tanaka, K., Takizawa, S., Setsuie, R., Sakurai, M., Sato, Y., Noda, M., Wada, K., 2004. Role of ubiquitin carboxy terminal hydrolase-L1 in neural cell apoptosis induced by ischemic retinal injury in vivo. Am. J. Pathol. 164, 59–64.

Ishitani, R., Tanaka, M., Sunaga, K., Katsube, N., Chuang, D.M., 1998. Nuclear localization of overexpressed glyceraldehyde-3-phosphate dehydrogenase in cultured cerebellar neurons undergoing apoptosis. Mol. Pharmacol. 53, 701–707.

Iwai, K., 2003. An ubiquitin ligase recognizing a protein oxidized by iron: implications for the turnover of oxidatively damaged proteins. J. Biochem. 134, 175–182.

Kabuta, T., Furuta, A., Aoki, S., Furuta, K., Wada, K., 2008. Aberrant interaction between Parkinson disease-associated mutant UCH-L1 and the lysosomal receptor for chaperone-mediated autophagy. J. Biol. Chem. 283, 23731–23738.

Kang, S.I., Choi, H.W., Kim, I.Y., 2008. Redox-mediated modification of PLZF by SUMO-1 and ubiquitin. Biochem. Biophys. Res. Commun. 369, 1209–1214.

Kikuchi, T., Mukoyama, M., Yamazaki, K., Moriya, H., 1990. Axonal degeneration of ascending sensory neurons in gracile axonal dystrophy mutant mouse. Acta Neuropathol. 80, 145–151.

Knowles, M.R., Cervino, S., Skynner, H.A., Hunt, S.P., de Felipe, C., Salim, K., Meneses-Lorente, G., McAllister, G., Guest, P.C., 2003. Multiplex proteomic analysis by two-dimensional differential in-gel electrophoresis. Proteomics 3, 1162–1171.

Kobayashi, A., Kang, M.I., Okawa, H., Ohtsuji, M., Zenke, Y., Chiba, T., Igarashi, K., Yamamoto, M., 2004. Oxidative stress sensor Keap1 functions as an adaptor for Cul3-based E3 ligase to regulate proteasomal degradation of Nrf2. Mol. Cell. Biol. 24, 7130–7139.

Larsen, C.N., Krantz, B.A., Wilkinson, K.D., 1998. Substrate specificity of deubiquitinating enzymes: ubiquitin C-terminal hydrolases. Biochemistry 37, 3358–3368.

Li, H., Li, S.H., Yu, Z.X., Shelbourne, P., Li, X.J., 2001. Huntingtin aggregate-associated axonal degeneration is an early pathological event in Huntington's disease mice. J. Neurosci. 21, 8473–8481.

Liu, Y., Fallon, L., Lashuel, H.A., Liu, Z., Lansbury Jr., P.T., 2002. The UCH-L1 gene encodes two opposing enzymatic activities that affect alpha-synuclein degradation and Parkinson's disease susceptibility. Cell 111, 209–218.

Miura, H., Oda, K., Endo, C., Yamazaki, K., Shibasaki, H., Kikuchi, T., 1993. Progressive degeneration of motor nerve terminals in GAD mutant mouse with hereditary sensory axonopathy. Neuropathol. Appl. Neurobiol. 19, 41–51.

Mukoyama, M., Yamazaki, K., Kikuchi, T., Tomita, T., 1989. Neuropathology of gracile axonal dystrophy (GAD) mouse. An animal model of central distal axonopathy in primary sensory neurons. Acta Neuropathol. 79, 294–299.

Nakajima, H., Amano, W., Fujita, A., Fukuhara, A., Azuma, Y.T., Hata, F., Inui, T., Takeuchi, T., 2007. The active site cysteine of the proapoptotic protein glyceraldehyde-3-phosphate dehydrogenase is essential in oxidative stress-induced aggregation and cell death. J. Biol. Chem. 282, 26562–26574.

Oda, K., Yamazaki, K., Miura, H., Shibasaki, H., Kikuchi, T., 1992. Dying back type axonal degeneration of sensory nerve terminals in muscle spindles of the gracile axonal dystrophy (GAD) mutant mouse. Neuropathol. Appl. Neurobiol. 18, 265–281.

Okada, K., Wangpoengtrakul, C., Osawa, T., Toyokuni, S., Tanaka, K., Uchida, K., 1999. 4-Hydroxy-2-nonenal-mediated impairment of intracellular proteolysis during oxidative stress. Identification of proteasomes as target molecules. J. Biol. Chem. 274, 23787–23793.

Osaka, H., Wang, Y.L., Takada, K., Takizawa, S., Setsuie, R., Li, H., Sato, Y., Nishikawa, K., Sun, Y.J., Sakurai, M., Harada, T., Hara, Y., Kimura, I., Chiba, S., Namikawa, K., Kiyama, H., Noda, M., Aoki, S., Wada, K., 2003. Ubiquitin carboxy-terminal hydrolase L1 binds to and stabilizes monoubiquitin in neuron. Hum. Mol. Genet. 12, 1945–1958.

Saigoh, K., Wang, Y.L., Suh, J.G., Yamanishi, T., Sakai, Y., Kiyosawa, H., Harada, T., Ichihara, N., Wakana, S., Kikuchi, T., Wada, K., 1999. Intragenic deletion in the gene encoding ubiquitin carboxy-terminal hydrolase in gad mice. Nat. Genet. 23, 47–51.

Sawa, A., Khan, A.A., Hester, L.D., Snyder, S.H., 1997. Glyceraldehyde-3-phosphate dehydrogenase: nuclear translocation participates in neuronal and nonneuronal cell death. Proc. Natl. Acad. Sci. U.S.A. 94, 11669–11674.

Sen, N., Hara, M.R., Kornberg, M.D., Cascio, M.B., Bae, B.I., Shahani, N., Thomas, B., Dawson, T.M., Dawson, V.L., Snyder, S.H., Sawa, A., 2008. Nitric oxide-induced nuclear GAPDH activates p300/CBP and mediates apoptosis. Nat. Cell. Biol. 10, 866–873.

Shaw, M.M., Riederer, B.M., 2003. Sample preparation for two-dimensional gel electrophoresis. Proteomics 3, 1408–1417.

Sirover, M.A., 1999. New insights into an old protein: the functional diversity of mammalian glyceraldehyde-3-phosphate dehydrogenase. Biochim. Biophys. Acta 1432, 159–184.

Stokin, G.B., Lillo, C., Falzone, T.L., Brusch, R.G., Rockenstein, E., Mount, S.L., Raman, R., Davies, P., Masliah, E., Williams, D.S., Goldstein, L.S., 2005. Axonopathy and transport deficits early in the pathogenesis of Alzheimer's disease. Science 307, 1282–1288.

Wang, Y.L., Takeda, A., Osaka, H., Hara, Y., Furuta, A., Setsuie, R., Sun, Y.J., Kwon, J., Sato, Y., Sakurai, M., Noda, M., Yoshikawa, Y., Wada, K., 2004. Accumulation of beta- and gamma-synucleins in the ubiquitin carboxyl-terminal hydrolase L1-deficient gad mouse. Brain Res. 1019, 1–9.

Wilkinson, K.D., Lee, K.M., Deshpande, S., Duerksen-Hughes, P., Boss, J.M., Pohl, J., 1989. The neuron-specific protein PGP 9.5 is a ubiquitin carboxyl-terminal hydrolase. Science 246, 670–673.

Yamazaki, K., Wakasugi, N., Tomita, T., Kikuchi, T., Mukoyama, M., Ando, K., 1988. Gracile axonal dystrophy (GAD), a new neurological mutant in the mouse. Proc. Soc. Exp. Biol. Med. 187, 209–215.

Zheng, L., Roeder, R.G., Luo, Y., 2003. S phase activation of the histone H2B promoter by OCA-S, a coactivator complex that contains GAPDH as a key component. Cell 114, 255–266.

Journal of Neurochemistry

JNC

JOURNAL OF NEUROCHEMISTRY | 2011 | 116 | 76–81

doi: 10.1111/j.1471-4159.2010.07086.x

Polypyrimidine tract-binding protein 1 regulates the alternative splicing of dopamine receptor D_2

Toshikazu Sasabe,*† Eugene Futai* and Shoichi Ishiura*

*Department of Life Sciences, Graduate School of Arts and Sciences, The University of Tokyo, Tokyo, Japan

†Research Fellowships of the Japan Society for the Promotion of Science for Young Scientists

Abstract

Dopamine receptor D_2 (DRD2) has two splicing isoforms, a long form (D2L) and short form (D2S), which have distinct functions in the dopaminergic system. However, the regulatory mechanism of the alternative splicing of *DRD2* is unknown. In this study, we examined which splicing factors regulate the expression of D2L and D2S by over-expressing several RNA-binding proteins in HEK293 cells. In a cellular splicing assay, the over-expression of polypyrimidine tract-binding protein 1 (PTBP1) reduced the expression of D2S, whereas the knockdown of PTBP1 increased the expression of D2S. We also identified the regions of *DRD2* that are responsive to PTBP1 using heterologous minigenes and deletion mutants. Our results indicate that PTBP1 regulates the alternative splicing of *DRD2*. Considering that DRD2 inhibits cAMP-dependent protein kinase A, which modulates the intracellular localization of PTBP1, PTBP1 may contribute to the autoregulation of DRD2 by regulating the expression of its isoforms.

Keywords: alternative splicing, dopamine, dopamine receptor D_2, PTBP1.

J. Neurochem. (2011) **116**, 76–81.

Dopamine is the predominant neurotransmitter in the CNS, where it plays a leading role in the regulation of such physiological functions as locomotor activity, cognition, positive reinforcement, and hormone secretion. The effects of dopamine are mediated by its binding to five G-protein-coupled receptors, which are divided into two subclasses: D_1-like (D_1 and D_5) and D_2-like (D_2, D_3, and D_4). Dopamine receptor D_2 (DRD2) is the main autoreceptor of the dopaminergic system (Centonze *et al.* 2002); however, it is also critical for post-synaptic transmission (Usiello *et al.* 2000).

Alternative gene splicing generates two distinct isoforms of DRD2, a long form (D2L) and short form (D2S), which differ in the presence of a 29-amino-acid insert in the third cytoplasmic loop. D2L is expressed mainly in post-synaptic regions, whereas D2S is expressed mainly in pre-synaptic regions (Khan *et al.* 1998; Usiello *et al.* 2000). These isoforms differentially contribute to the pre-synaptic inhibition of glutamate and GABA transmission (Centonze *et al.* 2004); moreover, they exhibit specific G_i protein preferences (Senogles 1994; Guiramand *et al.* 1995; Senogles *et al.* 2004) and have distinct roles in the regulation of protein phosphorylation (Lindgren *et al.* 2003). Furthermore, behavioral studies of D2L-deficient mice have shown that D2L and D2S contribute differentially to the regulation of certain motor functions (Usiello *et al.* 2000; Wang *et al.* 2000) and emotional responses (Hranilovic *et al.* 2008). Similarly, human genetic studies have shown that the intronic single nucleotide polymorphism rs1076560, which has a significant effect on the expression ratio of the DRD2 isoforms, is associated with cognitive processing (Zhang *et al.* 2007) and emotional processing (Blasi *et al.* 2009). These results suggest that the expression ratio of the DRD2 isoforms is important for their functions.

However, little is known about the regulatory mechanism that mediates the alternative splicing of *DRD2*. Although it has been reported that haloperidol, sex steroid hormones, and ethanol affect the expression of splice variants (Arnauld *et al.* 1991; Guivarc'h *et al.* 1995, 1998; Oomizu *et al.* 2003), the molecular basis for these differences is unclear. In general, changes in splicing patterns are directed by regula-

Received August 26, 2010; revised manuscript received October 18, 2010; accepted October 22, 2010.

Address correspondence and reprint requests to Dr Shoichi Ishiura, Department of Life Sciences, Graduate School of Arts and Sciences, The University of Tokyo, 3-8-1, Komaba, Meguro-ku, Tokyo 153-8902, Japan. E-mail: cishiura@mail.ecc.u-tokyo.ac.jp

Abbreviations used: D2L, long form of DRD2; D2S, short form of DRD2; DRD2, dopamine receptor D_2; nPTB, neural PTB; PTBP1, polypyrimidine tract-binding protein 1; Tpm2, tropomyosin 2.

tory proteins that bind the pre-mRNA sequence and enhance or silence particular splicing choices (Li *et al.* 2007). Thus, in this study, we searched for proteins that regulate the alternative splicing of *DRD2* using a cellular splicing assay and identified the involvement of the splicing factor polypyrimidine tract-binding protein 1 (PTBP1).

Materials and methods

Plasmid construction

The region from exon 5 to exon 7 of *DRD2* was amplified from human genomic DNA and cloned into the *Xho*I-*Hind*III site of pEYFP-C1 (Clontech, Mountain View, CA, USA) (Fig. 1a). The open reading frames that encode SF2/ASF, PTBP1, nPTB, NOVA1, HuB, FOX2, hnRNP A1, and Tra2b were amplified by PCR from a human fetal brain cDNA library (Clontech) and cloned into pcDNA3.1/V5-His (Invitrogen, Carlsbad, CA, USA) using conventional biological techniques. Primer sequences are listed in Table S1. Plasmid constructions of NAPOR and FOX1 are gifts from Dr. Yoshihiro Kino, RIKEN Brain Science Institute, and hnRNP H from Dr. Kinji Ohno, Nagoya University. Heterologous minigenes were generated by inserting *DRD2* fragments containing exon 6, exon 7 and flanking regions into pEGFP-Tpm2-ex1-2 (a gift from Dr. Kino, RIKEN Brain Science Institute). *DRD2* deletion mutants were generated by inverse PCR from the wild-type plasmid using primers flanking the deleted regions. The nucleotide sequences of the DNA inserts were confirmed by sequencing.

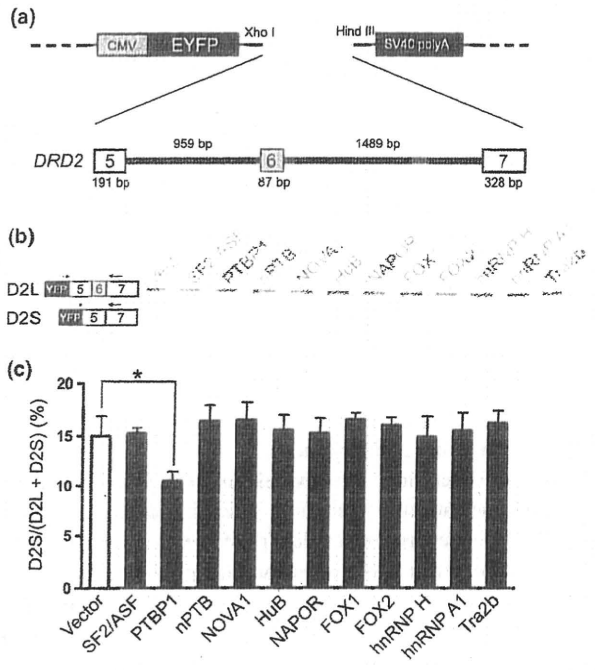

Fig. 1 The over-expression of PTBP1 reduced the alternative splicing of D2S. (a) Structure of the *DRD2* minigene. (b) Representative result from RT-PCR assays in which the *DRD2* minigene and plasmids for expressing RNA-binding proteins were transfected into HEK293 cells. The upper bands correspond to the splice product containing exon 6 (D2L), while the lower bands correspond to the splice product lacking exon 6 (D2S). (c) Bar chart showing the quantified percentage of D2S (Mean + SEM, $n = 3$). The statistical significance was analyzed by Dunnett's multiple-comparison test (*$p < 0.05$).

Cell culture and transfection

HEK293 and SH-SY5Y cells were cultured in Dulbecco's modified Eagle's medium supplemented with 10% (v/v) fetal bovine serum and incubated at 37°C with 5% CO_2. For the minigene assays, HEK293 cells were transfected with plasmids for the expression of minigene and V5-tagged proteins using Fugene 6 (Roche Diagnostics, Basel, Switzerland). In our RNAi experiments, HEK293 cells were transfected with the minigene plasmids and an siRNA for *PTBP1* (Invitrogen, Stealth™ Select RNAi HSS143520, and Negative Control Hi GC) and *nPTB* (Invitrogen, Stealth™ Select RNAi HSS126818, and Negative Control Lo GC) using Lipofectamine 2000 (Invitrogen), and SH-SY5Y cells were transfected with the siRNA using Lipofectamine RNAiMAX (Invitrogen) and the Reverse Transfection protocol. The efficacy of the RNAi-mediated knockdown of endogenous PTBP1, nPTB, and actin expressions was determined by western blot analysis using anti-PTBP1 (Invitrogen, catalog No. 32-4800), anti-nPTB (Abnova, Taipei City, Taiwan, catalog No. H00058155-A01), and anti-actin (Sigma-Aldrich, St. Louis, MO, USA, catalog No. A2066) antibodies.

Identification of DRD2 splice variants

Forty-eight hours after transfection, total RNA was isolated from the cells using a GenElute Mammalian Total RNA Miniprep Kit (Sigma-Aldrich). cDNA synthesis was performed using a PrimeScript First Strand cDNA Synthesis Kit (TAKARA BIO, Shiga, Japan) using oligo dT primer. The DRD2 minigene fragments were amplified by PCR (20 cycles) using a forward primer specific for the 3′ region of *EYFP* (AAGTCCGGACTCAGATCTCG) and a *DRD2*-specific reverse primer (DRD2-Ex7-Rv) that annealed to the 5′ region of exon 7 (CATCTCCATCTCCAGCTCCT). To detect endogenous *DRD2* fragments, a forward primer specific for exons 4 and 5 (CAATAACGCAGACCAGAACG) and DRD2-Ex7-Rv were used (40 cycles). For tropomyosin 2 (Tpm2)-based minigenes, primers green fluorescence protein (GFP)-Fw (CATGGTCCTGCTGGAGTTCGTG) and Tpm2-ex2-splicing-Rv2 (GGAGGGCCTGCTGCTCTTC) were used (Kino *et al.* 2009). The amplified products were resolved by 6% polyacrylamide gel electrophoresis and visualized using ethidium bromide. The intensities of the bands corresponding to the long and short forms were quantified by LAS-3000 and MultiGage software (Fuji Film, Tokyo, Japan). The quantified values were divided by the number of base pairs.

Results

PTBP1 regulates the alternative splicing of DRD2

To identify trans-acting factors that regulate the alternative splicing of *DRD2*, we used RT-PCR to detect splice variants. We constructed a gene fragment encompassing exons 5 through 7 of human *DRD2* in the vector pEYFP (Fig. 1a). This minigene was then transfected into HEK293 cells, and the expression ratios of D2L and D2S were analyzed by

RT-PCR. When the *DRD2* minigene was transfected with empty pcDNA3.1, the percentage of D2S was about 15% (Fig. 1b and c). Next, we expressed V5-tagged versions of several proteins known to regulate pre-mRNA splicing in the nervous system (SF2/ASF, PTBP1, nPTB, NOVA1, HuB, NAPOR, FOX1, FOX2, hnRNP H, hnRNP A1, and Tra2b); notably, SF2/ASF was previously proposed to regulate the alternative splicing of *DRD2* (Oomizu *et al.* 2003). Among the proteins tested, only when PTBP1 was transfected with the *DRD2* minigene was the percentage of D2S significantly reduced (to about 10%; Fig. 1b and c). We have confirmed the expressions of each RNA-binding proteins by western blot analysis and noted that the abundance of nPTB, NAPOR, and FOX1 are low (Figure S1). In addition, we showed the effects of PTBP1 were concentration dependent (Figure S2).

Next, we knocked down endogenous PTBP1 expression using an siRNA to confirm the effect of PTBP1 on *DRD2* splicing. We first confirmed the efficacy of the siRNA in modulating the expression of the target protein by western blot analysis (Fig. 2b). The presence of two PTBP1 bands rather than one is most likely because of phosphorylation. (Grossman *et al.* 1998). When the *DRD2* minigene was transfected with an siRNA for *PTBP1*, the percentage of D2S was significantly increased compared to transfection with a control siRNA (Fig. 2a). We also examined the effect of the knockdown of nPTB, a homologue of PTBP1, because it was reported that appearance of some exons are affected by both PTBP1 and nPTB (Boutz *et al.* 2007). The knockdown of PTBP1 increased the expression of nPTB (Fig. 2b), consistent with the previous reports (Boutz *et al.* 2007; Makeyev *et al.* 2007). While endogenous nPTB level was remarkably low and the knockdown of nPTB by siRNA was not observed, the increase in nPTB expression by the knockdown of PTBP1 was clearly inhibited by a siRNA for nPTB (Fig. 2b). Even when the increase in nPTB was inhibited, the knockdown of PTBP1 still increased the production of D2S splice variant (Fig. 2a), suggesting that the increase in nPTB has little or no effect on the alternative splicing of DRD2. Furthermore, we examined whether PTBP1 regulates the alternative splicing of endogenous *DRD2* in human neuroblastoma SH-SY5Y cells. When the siRNA for *PTBP1* was transfected into SH-SY5Y cells, the percentage of endogenous D2S fragments was also increased (Fig. 2c and d).

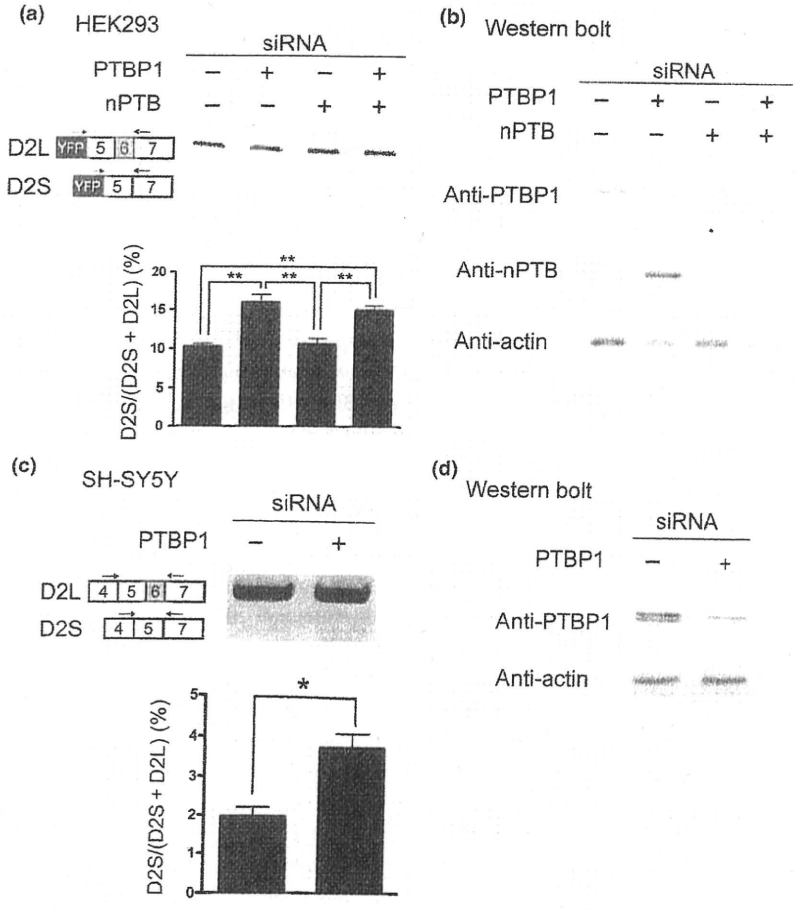

Fig. 2 The knockdown of PTBP1 increased the production of D2S splice variant. (a) Representative result from our cellular splicing assay using the *DRD2* minigene and siRNA for *PTBP1* and *nPTB* in HEK293 cells. Bar charts show the quantified percentages of D2S (Mean + SEM, $n = 3$). The statistical significances were analyzed using Tukey's multiple comparison test (**$p < 0.01$). (b) Representative result of western blot analysis of PTBP1 and nPTB in HEK293 cells. (c) Representative result of endogenous *DRD2* splicing using a siRNA for *PTBP1* in SH-SY5Y cells. Bar charts show the quantified percentages of D2S (Mean + SEM, $n = 3$). The statistical significance was analyzed using *t*-tests (*$p < 0.05$). (d) Representative result of western blot analysis of PTBP1 in SH-SY5Y cells.

Intronic regions flanking exon 6 are required for the PTBP1-mediated regulation of DRD2 splicing

To define the regions of *DRD2* that are required for its regulation by PTBP1, we utilized several previously generated heterologous minigenes (Kino *et al.* 2009). In these minigenes, the regions of interest were inserted in the context of constitutive exons of mouse *Tpm2*, which is distinct from *DRD2*. A reference fragment containing exon 9 of *Tpm2* and its flanking intronic regions or a *DRD2* fragment containing exon 6 or exon 7 and their flanking regions were inserted into a *Tpm2* fragment covering exons 1 and 2 (Fig. 3a). First, we

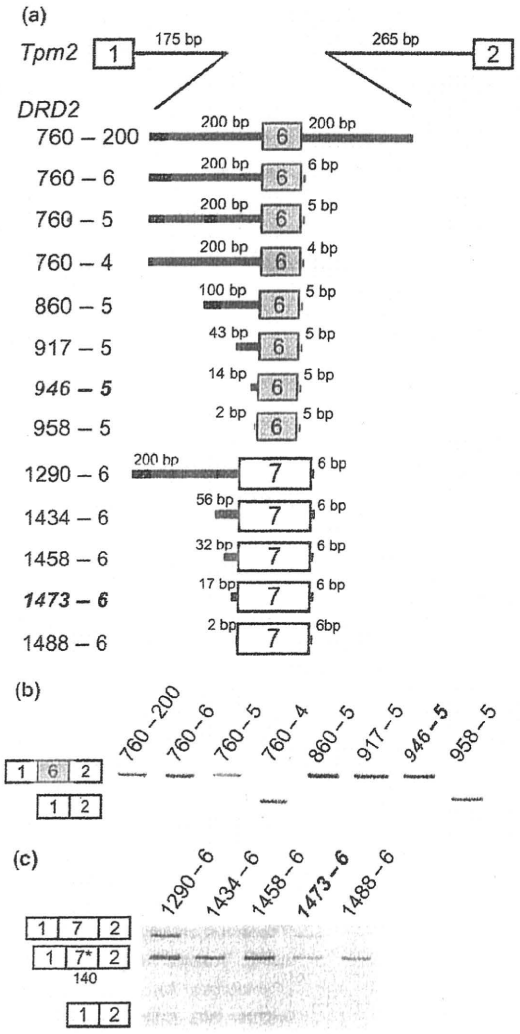

Fig. 3 Identification of DRD2 intronic regions which are necessary for the splicing of exon 6 and exon 7. (a) Structure of the *Tpm2*-based heterologous minigenes. The positions of the inserted nucleotides in introns 5, 6 and 7, as well as the numbers of base pairs in the fragments, are indicated. (b, c) Representative results from identification of splice variants using *Tpm2*-based heterologous minigenes in HEK293 cells. The white box 7* shows a shorter exon 7 lacking the first 140 nucleotides.

predicted branch sites by a web-based program called ESEfinder 3.0 (Table S2, http://rulai.cshl.edu/cgi-bin/tools/ESE3/esefinder.cgi). Then, using our *Tpm2*-based heterologous minigenes, we found that 14 bp upstream and 5 bp downstream of exon 6 are necessary for proper splicing (Fig. 3b). When exon 7 of DRD2 was inserted into Tpm2 cassette, a shorter exon 7 lacking the first 140 nucleotides was the main product. It was shown that 17 bp upstream of exon 7 is necessary for the splicing of full-length exon 7 (Fig. 3c). Because the primary elements regulating alternative splicing are thought to be located up to 200–300 nucleotides upstream and/or downstream of the regulated exon (Cooper 2005), a *DRD2* fragment stretching from 200 bp upstream of exon 6 (760 bp downstream of exon 5) to 200 bp downstream of exon 6 was used to examine the binding sequence of PTBP1 (Fig. 4a). PTBP1 had no effect on the inclusion of *Tpm2* exon 9 in HEK293 cells (Fig. 4b, left). In contrast, PTBP1 repressed *DRD2* exon 6 inclusion of the heterologous minigene, demonstrating that the inserted fragment of *DRD2* was sufficient for the response to PTBP1 (Fig. 4b, right). Next, to examine which region is necessary for the gene's responsiveness to PTBP1, we constructed *DRD2* deletion mutants lacking 200 bp upstream of exon 6 (Δint5_760–945), downstream of exon 6 (Δint6_6–200) or upstream of exon 7 (Δint6_1290–1487) (Fig. 4c). These deletion mutants were designed to include the regions that are necessary for splicing of exon 6 and exon 7. As shown in Fig. 4(d), Δint5_760–945 and Δint6_6–200 mutations altered the basal splicing pattern. Both deletion mutants exhibited markedly increased exclusion of exon 6 (from 15% to about 60% with vector transfection), suggesting the presence of elements in the deleted regions that enhance the inclusion of exon 6. Further, the over-expression of PTBP1 had no effect on either deletion mutant, indicating that both mutants had impaired responsiveness to PTBP1 (Fig. 4d). On the other hand, the over-expression of PTBP1 reduced D2S in the Δint6_1290–1487 mutant as well as a wild-type minigene, suggesting that PTBP1 affects the alternative splicing of DRD2 in regions other than the 3′ end of intron 6.

Discussion

Previous studies have shown that the functions of two splice variants of DRD2, D2L and D2S, differ in their biochemical properties and physiological functions (Senogles 1994; Guiramand *et al.* 1995; Khan *et al.* 1998; Usiello *et al.* 2000; Wang *et al.* 2000; Centonze *et al.* 2002, 2004; Lindgren *et al.* 2003; Senogles *et al.* 2004; Hranilovic *et al.* 2008); however, it is unclear what regulates the expression ratio of these isoforms. In this study, we identified PTBP1 as a splicing regulatory protein that reduces the expression of the D2S isoform.

Among the eleven proteins that we over-expressed with the *DRD2* minigene in HEK293 cells, only PTBP1

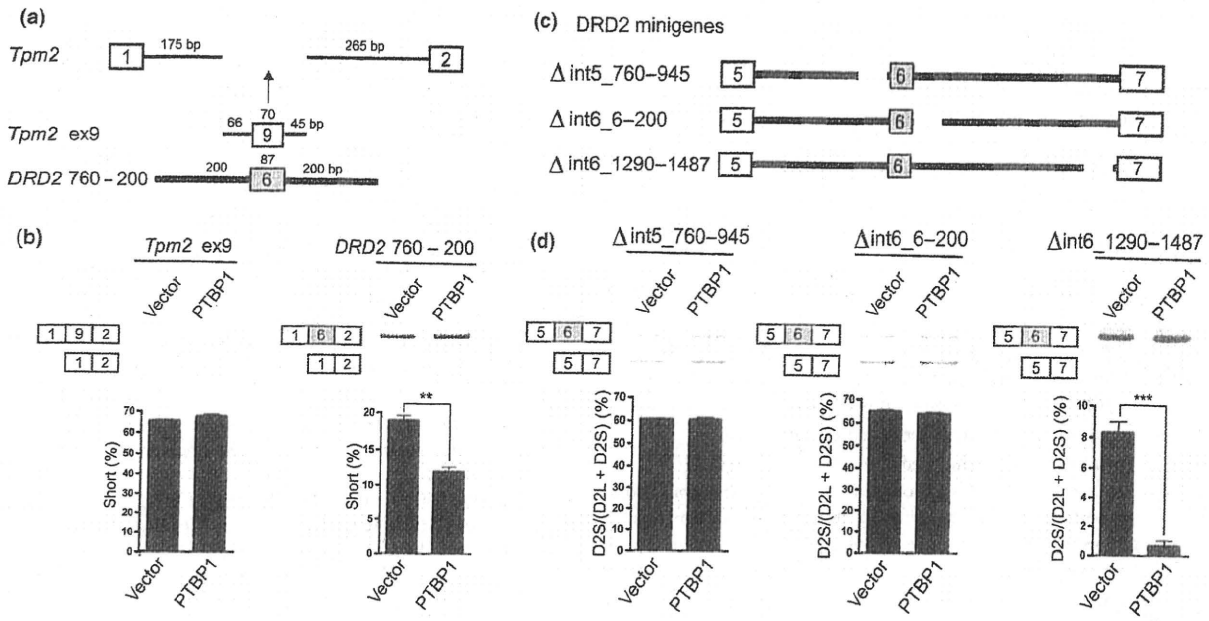

Fig. 4 Splicing regulation by PTBP1 in heterologous minigenes and *DRD2* deletion mutants. (a) Structure of the *Tpm2*-based heterologous minigene. Intronic fragments derived from *DRD2* are indicated by thick lines, whereas those derived from *Tpm2* are indicated by thin lines. (b) Splicing assay results using *Tpm2*-based heterologous minigenes and PTBP1 in HEK293 cells. Bar charts show the quantified percentages of exon exclusion (Mean + SEM, $n = 3$). (c) Structure of the *DRD2* deletion mutants. The positions of the inserted nucleotides in introns 5 and 6 are indicated. (d) Splicing assay results using the *DRD2* deletion mutants and PTBP1 in HEK293 cells. Bar charts show the quantified percentages of D2S (Mean + SEM, $n = 3$). The statistical significance was analyzed using *t*-tests (**$p < 0.01$, ***$p < 0.001$).

produced an altered splicing pattern (Fig. 1b and c). The reduction in the percentage of D2S suggests that PTBP1 enhances the inclusion of the alternative exon 6. Although the effect of PTBP1 was relatively small, this effect was shown to be concentration dependent (Figure S2). We also demonstrated that endogenous PTBP1 regulates DRD2 splicing by knockdown experiments in HEK293 cells with the *DRD2* minigene and in SH-SY5Y cells with the endogenous *DRD2* gene (Fig. 2a and c). Even though the effect of PTBP1 was statistically significant, it was quantitatively small in our splicing assay. Therefore, some other splicing factors may be involved in the splicing regulation of *DRD2*. In addition, the double knockdown of PTBP1 and nPTB suggested that nPTB, a homolog of PTBP1, has little or no effect on the alternative splicing of DRD2 (Fig. 2a). However, because the expression levels of exogenous and endogenous nPTB were remarkably lower than PTBP1 in HEK293 cells, it is still unclear whether nPTB regulates the splicing of DRD2.

Next, we identified the regions responsive to PTBP1, using *Tpm2*-based heterologous minigenes and *DRD2* deletion mutants. Using our heterologous minigenes, the splicing of a *DRD2* fragment containing exon 6 as well as 200 bp-upstream and -downstream intronic regions was altered by PTBP1 (Fig. 4b), similar to the results obtained using the *DRD2* minigene (Fig. 1b and c). In the *DRD2* deletion mutants, PTBP1 had no effect on the splicing of deletion mutants lacking exon 6-flanking regions in intron 5 or 6, whereas PTBP1 still affected the splicing of a deletion mutant lacking the 3′ end of intron 6 (Fig. 4d). These results indicate that exon 6-flanking regions are sufficient for the response to PTBP1, and that both regions in introns 5 and 6 are necessary.

Although PTBP1 is known to bind cytosine and uracil (CU)-rich intronic elements flanking an exon and repress splicing (Wagner and Garcia-Blanco 2001; Sharma *et al.* 2008), in this study PTBP1 appeared to enhance the inclusion of *DRD2* exon 6 rather than repressing the splicing from exon 5 to exon 7. It is noted that intron 5 contains UCUCU (849-853) and intron 6 contains UCUUUCU (32–38) sequences, but we have no evidence that PTBP1 directly binds the pre-mRNA of *DRD2*. Therefore it is possible that PTBP1 may indirectly affect the alternative splicing of *DRD2*.

It was reported that a DRD2 antagonist, haloperidol, increased the expression of D2S (Arnauld *et al.* 1991). The activation of DRD2 is coupled to the inhibition of adenylyl cyclase and cAMP-dependent protein kinase A, and cAMP-dependent protein kinase A has been shown to modulate the nucleocytoplasmic translocation of PTBP1 (Xie *et al.* 2003; Knoch *et al.* 2006). Together with these reports, our results suggest that DRD2 regulates the expression of its isoforms by modulating the localization of PTBP1.

Acknowledgements

This work was supported in part by the Human Frontier Science Program and by a Grant-in-Aid from the Ministry of Education, Culture, Sports, Science and Technology of Japan to S.I. T.S. is supported by a JSPS Research Fellowship for Young Scientists. We thank Dr. Yoshihiro Kino for Tpm2 minigene.

Supporting information

Additional Supporting information may be found in the online version of this article:

Figure S1. The expressions of RNA-binding proteins were confirmed by western blot analysis.

Figure S2. The concentration dependency of the PTBP1 effects.

Table S1. Primer sequences used for cloning.

Table S2. Branch site prediction by ESEfinder 3.0.

As a service to our authors and readers, this journal provides supporting information supplied by the authors. Such materials are peer-reviewed and may be re-organized for online delivery, but are not copy-edited or typeset. Technical support issues arising from supporting information (other than missing files) should be addressed to the authors.

References

Arnauld E., Arsaut J. and Demotes-Mainard J. (1991) Differential plasticity of the dopaminergic D2 receptor mRNA isoforms under haloperidol treatment, as evidenced by in situ hybridization in rat anterior pituitary. *Neurosci. Lett.* **130**, 12–16.

Blasi G., Lo Bianco L., Taurisano P. *et al.* (2009) Functional variation of the dopamine D2 receptor gene is associated with emotional control as well as brain activity and connectivity during emotion processing in humans. *J. Neurosci.* **29**, 14812–14819.

Boutz P., Stoilov P., Li Q. *et al.* (2007) A post-transcriptional regulatory switch in polypyrimidine tract-binding proteins reprograms alternative splicing in developing neurons. *Genes Dev.* **21**, 1636–1652.

Centonze D., Usiello A., Gubellini P., Pisani A., Borrelli E., Bernardi G. and Calabresi P. (2002) Dopamine D2 receptor-mediated inhibition of dopaminergic neurons in mice lacking D2L receptors. *Neuropsychopharmacology* **27**, 723–726.

Centonze D., Gubellini P., Usiello A. *et al.* (2004) Differential contribution of dopamine D2S and D2L receptors in the modulation of glutamate and GABA transmission in the striatum. *Neuroscience* **129**, 157–166.

Cooper T. A. (2005) Use of minigene systems to dissect alternative splicing elements. *Methods* **37**, 331–340.

Grossman J., Meyer M., Wang Y., Mulligan G., Kobayashi R. and Helfman D. (1998) The use of antibodies to the polypyrimidine tract binding protein (PTB) to analyze the protein components that assemble on alternatively spliced pre-mRNAs that use distant branch points. *RNA* **4**, 613–625.

Guiramand J., Montmayeur J., Ceraline J., Bhatia M. and Borrelli E. (1995) Alternative splicing of the dopamine D2 receptor directs specificity of coupling to G-proteins. *J. Biol. Chem.* **270**, 7354–7358.

Guivarc'h D., Vernier P. and Vincent J. (1995) Sex steroid hormones change the differential distribution of the isoforms of the D2 dopamine receptor messenger RNA in the rat brain. *Neuroscience* **69**, 159–166.

Guivarc'h D., Vincent J. and Vernier P. (1998) Alternative splicing of the D2 dopamine receptor messenger ribonucleic acid is modulated by activated sex steroid receptors in the MMQ prolactin cell line. *Endocrinology* **139**, 4213–4221.

Hranilovic D., Bucan M. and Wang Y. (2008) Emotional response in dopamine D2L receptor-deficient mice. *Behav. Brain Res.* **195**, 246–250.

Khan Z., Mrzljak L., Gutierrez A., de la Calle A. and Goldman-Rakic P. (1998) Prominence of the dopamine D2 short isoform in dopaminergic pathways. *Proc. Natl Acad. Sci. USA* **95**, 7731–7736.

Kino Y., Washizu C., Oma Y., Onishi H., Nezu Y., Sasagawa N., Nukina N. and Ishiura S. (2009) MBNL and CELF proteins regulate alternative splicing of the skeletal muscle chloride channel CLCN1. *Nucleic Acids Res.* **37**, 6477–6490.

Knoch K., Meisterfeld R., Kersting S., Bergert H., Altkrüger A., Wegbrod C., Jäger M., Saeger H. and Solimena M. (2006) cAMP-dependent phosphorylation of PTB1 promotes the expression of insulin secretory granule proteins in beta cells. *Cell Metab.* **3**, 123–134.

Li Q., Lee J. and Black D. (2007) Neuronal regulation of alternative pre-mRNA splicing. *Nat. Rev. Neurosci.* **8**, 819–831

Lindgren N., Usiello A., Goiny M., Haycock J., Erbs E., Greengard P., Hokfelt T., Borrelli E. and Fisone G. (2003) Distinct roles of dopamine D2L and D2S receptor isoforms in the regulation of protein phosphorylation at presynaptic and postsynaptic sites. *Proc. Natl Acad. Sci. USA* **100**, 4305–4309.

Makeyev E., Zhang J., Carrasco M. and Maniatis T. (2007) The microRNA miR-124 promotes neuronal differentiation by triggering brain-specific alternative pre-mRNA splicing. *Mol. Cell* **27**, 435–448.

Oomizu S., Boyadjieva N. and Sarkar D. (2003) Ethanol and estradiol modulate alternative splicing of dopamine D2 receptor messenger RNA and abolish the inhibitory action of bromocriptine on prolactin release from the pituitary gland. *Alcohol. Clin. Exp. Res.* **27**, 975–980.

Senogles S. (1994) The D2 dopamine receptor isoforms signal through distinct Gi alpha proteins to inhibit adenylyl cyclase. A study with site-directed mutant Gi alpha proteins. *J. Biol. Chem.* **269**, 23120–23127.

Senogles S., Heimert T., Odife E. and Quasney M. (2004) A region of the third intracellular loop of the short form of the D2 dopamine receptor dictates Gi coupling specificity. *J. Biol. Chem.* **279**, 1601–1606.

Sharma S., Kohlstaedt L., Damianov A., Rio D. and Black D. (2008) Polypyrimidine tract binding protein controls the transition from exon definition to an intron defined spliceosome. *Nat. Struct. Mol. Biol.* **15**, 183–191.

Usiello A., Baik J., Rougé-Pont F., Picetti R., Dierich A., LeMeur M., Piazza P. and Borrelli E. (2000) Distinct functions of the two isoforms of dopamine D2 receptors. *Nature* **408**, 199–203.

Wagner E. and Garcia-Blanco M. (2001) Polypyrimidine tract binding protein antagonizes exon definition. *Mol. Cell. Biol.* **21**, 3281–3288.

Wang Y., Xu R., Sasaoka T., Tonegawa S., Kung M. and Sankoorikal E. (2000) Dopamine D2 long receptor-deficient mice display alterations in striatum-dependent functions. *J. Neurosci.* **20**, 8305–8314.

Xie J., Lee J., Kress T., Mowry K. and Black D. (2003) Protein kinase A phosphorylation modulates transport of the polypyrimidine tract-binding protein. *Proc. Natl Acad. Sci. USA* **100**, 8776–8781.

Zhang Y., Bertolino A., Fazio L. *et al.* (2007) Polymorphisms in human dopamine D2 receptor gene affect gene expression, splicing, and neuronal activity during working memory. *Proc. Natl Acad. Sci. USA* **104**, 20552–20557.